Enhancement of plume dilution in two-dimensional and three-dimensional porous media by flow focusing in high-permeability inclusions

Ye, Yu; Chiogna, Gabriele; Cirpka, Olaf A.; Grathwohl, Peter; Rolle, Massimo

Published in:
Water Resources Research

Link to article, DOI:
10.1002/2015wr016962

Publication date:
2015

Document Version
Publisher's PDF, also known as Version of record

AGU PUBLICATIONS

Water Resources Research

RESEARCH ARTICLE
10.1002/2015WR016962

Key Points:
- Experimental theoretical and numerical study of flow focusing and dilution
- Mixing enhancement analyzed in 2-D and 3-D heterogeneous flow-through systems
- Mixing enhancement depends on system dimensionality, inclusions position and D_t

Supporting Information:
- Supporting Information S1

Correspondence to:
M. Rolle,
masro@env.dtu.dk

Citation:
Ye, Y., G. Chiogna, O. A. Cirpka, P. Grathwohl, and M. Rolle (2015), Enhancement of plume dilution in two-dimensional and three-dimensional porous media by flow focusing in high-permeability inclusions, *Water Resour. Res.*, *51*, doi:10.1002/2015WR016962.

Received 20 JAN 2015
Accepted 23 JUN 2015
Accepted article online 03 JULY 2015

Enhancement of plume dilution in two-dimensional and three-dimensional porous media by flow focusing in high-permeability inclusions

Yu Ye[1], Gabriele Chiogna[1,2], Olaf A. Cirpka[1], Peter Grathwohl[1], and Massimo Rolle[1,3]

[1]Center for Applied Geoscience, University of Tübingen, Tübingen, Germany, [2]Faculty of Civil, Geo and Environmental Engineering, Technical University of Munich, Munich, Germany, [3]Department of Environmental Engineering, Technical University of Denmark, Lyngby, Denmark

Abstract In porous media, lateral mass exchange exerts a significant influence on the dilution of solute plumes in quasi steady state. This process is one of the main mechanisms controlling transport of continuously emitted conservative tracers in groundwater and is fundamental for the understanding of many degradation processes. We investigate the effects of high-permeability inclusions on transverse mixing in three-dimensional versus two-dimensional systems by experimental, theoretical, and numerical analyses. Our results show that mixing enhancement strongly depends on the system dimensionality and on the parameterization used to model transverse dispersion. In particular, no enhancement of transverse mixing would occur in three-dimensional media if the local transverse dispersion coefficient was uniform and flow focusing in both transverse directions was identical, which is fundamentally different from the two-dimensional case. However, the velocity and grain size dependence of the transverse dispersion coefficient and the correlation between hydraulic conductivity and grain size lead to prevailing mixing enhancement within the inclusions, regardless of dimensionality. We perform steady state bench-scale experiments with multiple tracers in three-dimensional and quasi two-dimensional flow-through systems at two different velocities (1 and 5 m/d). We quantify transverse mixing by the flux-related dilution index and compare the experimental results with model simulations. The experiments confirm that, although dilution is larger in three-dimensional systems, the enhancement of transverse mixing due to flow focusing is less effective than in two-dimensional systems. The spatial arrangement of the high-permeability inclusions significantly affects the degree of mixing enhancement. We also observe more pronounced compound-specific effects in the dilution of solute plumes in three-dimensional porous media than in two-dimensional ones.

1. Introduction

Groundwater flow in natural aquifers is characterized by low flow velocities [10^{-3} to 10^{1} m/d, e.g., *Fetter*, 2000], leading to rather small transverse hydrodynamic dispersion coefficients [10^{-11} to 10^{-8} m^2/s, e.g., *Bear*, 1972] and thus rather inefficient transverse mixing [e.g., *Davis et al*., 1999; *Prommer et al*., 2006; *van der Kamp et al*., 1994]. This is a key factor for understanding the fate and transport of widespread contaminants in groundwater, including compounds released from NAPL spills or leaking landfills. In these cases, the contaminants are continuously emitted from the source over typical time scales of decades and the released plumes approach steady state conditions determined by the dynamic equilibrium between the contaminant mass released at the source and its destruction by degradation processes [e.g., *Mace et al*., 1997; *Wiedemeier et al*., 1999]. Under these conditions, the reaction of continuously emitted pollutants with dissolved reactants in the ambient groundwater is typically controlled by transverse dispersive mixing [e.g., *Anneser et al*., 2008; *Cirpka et al*., 1999; *Ham et al*., 2004; *Knutson et al*., 2007; *Mayer et al*., 2001; *Prommer et al*., 2009; *Thornton et al*., 2001], although shearing and longitudinal dispersion can play an important role at the front of the plume. Transverse mixing represents the key process in estimating the length of steady state contaminant plumes [e.g., *Cirpka et al*., 2012; *Liedl et al*., 2005, 2011; *Maier and Grathwohl*, 2006; *Zarlenga and Fiori*, 2013, 2014]. In transient transport, local lateral mass exchange controls the transition of longitudinal plume spreading to dilution [*Kitanidis*, 1994], the coalescence of plume lamellae within heterogeneous domains [e.g., *Le Borgne et al*., 2013], and is critical in interpreting solute breakthrough curves [e.g., *Pedretti et al*., 2013; *Rolle and Kitanidis*, 2014].

The heterogeneity of porous media can sustain concentration gradients by deforming the plume boundary, enhancing therefore diffusive fluxes [e.g., *Cirpka et al*., 2012; *Rolle et al*., 2009; *Werth et al*., 2006]. Flow focusing in high-permeability zones squeezes streamlines in narrow regions of the domain, thus increasing concentration gradients of the solutes in the direction transverse to the streamlines. In two-dimensional systems, the increase in concentration gradients caused by flow focusing prevails over the decrease of transport time in such regions, thus leading to a net enhancement of transverse mixing [e.g., *Chiogna et al*., 2011a; *Cirpka et al*., 2011; *Werth et al*., 2006; *Willingham et al*., 2008]. The role of this process is particularly relevant for degradation reactions occurring at the narrow fringe of contaminant plumes where reactants can physically mix [e.g., *Anneser et al*., 2008; *Bauer et al*., 2009; *Bjerg et al*., 2011; *Cirpka et al*., 2006; *Lerner et al*., 2000].

Due to the small spatial scale at which mixing occurs, resolving steep concentration gradients at the field scale remains challenging despite the rapid development of improved monitoring techniques [e.g., *Annable et al*., 2005; *Anneser et al*., 2008; *Devlin et al*., 2012]. Therefore, laboratory experiments [e.g., *Castro-Alcala et al*., 2012; *de Anna et al*., 2014; *Haberer et al*., 2015; *Rolle et al*., 2013a] and numerical simulations at multiple scales [e.g., *de Dreuzy et al*., 2012; *Herrera and Valocchi*, 2006; *Hochstetler et al*., 2013; *Porta et al*., 2013; *Rolle et al*., 2013b; *Tartakovsky et al*., 2009] are fundamental for the understanding of dilution in porous media. Most of these studies, however, focused on (quasi) two-dimensional systems, while detailed experimental and modeling investigations in three-dimensional domains are less common [e.g., *Herrera et al*., 2010; *Rashidi et al*., 1996; *Silliman*, 1996; *Yoon and McKenna*, 2012; *Cirpka et al*., 2015]. In particular, few experimental studies have been performed to investigate solute transport in fully three-dimensional porous media. Such studies have mostly focused on the development of noninvasive techniques to map solute concentrations and on the investigation of solute breakthrough [e.g., *Chen et al*., 2002; *Danquigny et al*., 2004; *Marica et al*., 2011; *Oswald et al*., 1997; *Oswald and Kinzelbach*, 2004], whereas systematic experimental studies on transverse mixing in fully three-dimensional systems are scarce.

Cirpka et al. [2015] proposed three mechanisms by which three-dimensional heterogeneity enhances transverse mixing: (a) flow focusing, which is the main transverse-mixing enhancing process in two-dimensional steady state transport, (b) depth-dependent plume meandering leading to an enlarged surface area of the plume, and (c) twisting streamlines caused by spatially variable anisotropy. The present contribution exclusively addresses the first mechanism, providing theoretical analyses, numerical results, and an experimental validation. In contrast to the other two processes, transverse mixing enhancement by flow focusing can occur both in 2-D and 3-D setups thus allowing for a clear comparison on the effects of such mechanism in two and three dimensions. Effects of transient flow on transverse mixing in heterogeneous media [e.g., *Cirpka and Attinger*, 2003; *Dentz and Carrera*, 2003], which are difficult to address by experiments, are not considered in the present study.

Laboratory bench-scale experiments greatly simplify natural aquifers and cannot capture the complex arrangements of heterogeneous anisotropic materials [e.g., *Heinz and Aigner*, 2003], the hydraulic connectivity of high-permeability inclusions [e.g., *Renard and Allard*, 2013; *Pedretti et al*., 2013], as well as the chemical and biogeochemical complexity of natural aquifer systems. However, flow-through laboratory experiments allow the detailed investigation of selected processes under well-defined and controlled conditions. They advance process understanding and allow testing conceptual and numerical models against experimental data affected by significantly less uncertainty than field observations.

In this work, we aim at analyzing the effects of physical heterogeneity, with a very simplified geometrical and topological structure, on dilution and its enhancement under steady state transport conditions in three-dimensional setups. In particular, we investigate the enhancement of transverse mixing caused by flow focusing in high-permeability inclusions, comparing two-dimensional and three-dimensional laboratory flow-through systems. We performed conservative multitracer experiments at two velocities (1 and 5 m/d). Three heterogeneous setups were considered in the three-dimensional experiments. We performed also a multitracer experiment reproducing a cross section of one of the aforementioned setups in a quasi two-dimensional system. We measured solute mass fluxes with high-spatial resolution at the outlet of the flow-through chambers. We quantify dilution of the steady state plumes by the flux-related dilution index [*Rolle et al*., 2009] and derive an analytical solution of the mixing-enhancement factor for the 3-D case, extending the 2-D analysis performed by *Werth et al*. [2006]. A model-based interpretation of the

experimental results allows quantifying the amount of mixing enhancement due to flow focusing in comparison to the homogeneous case.

The main objectives of this study are to (i) investigate steady state plume dilution by transverse mixing in fully 3-D flow-through systems with high-permeability inclusions; (ii) quantify the mixing enhancement by flow focusing in the inclusions in the 3-D setups and compare it with the effects observed in (quasi) 2-D systems; (iii) assess how the parameterization of transverse dispersion and compound-specific properties of different solutes affect the enhancement of dilution in high-permeability inclusions of three-dimensional porous media.

2. Theory

2.1. Governing Flow and Transport Equations

Flow in porous media can be described by combining the continuity equation and Darcy's law. The latter can be written as

$$\mathbf{q}(\mathbf{x}) = -\mathbf{K}(\mathbf{x}) \cdot \nabla \phi(\mathbf{x}) \tag{1}$$

where $\mathbf{q}$ [$L\ T^{-1}$] is the specific-discharge vector, $\mathbf{x}$ [L] denotes the vector of spatial coordinates, $\mathbf{K}$ [$L\ T^{-1}$] is the hydraulic conductivity tensor, which depends on water saturation, and ϕ [L] is the hydraulic-head field. In this study, we consider the case of an isotropic porous medium, so that $\mathbf{K}$ is a scalar field. While the main focus is on groundwater, where water saturation is unity, we include the unsaturated zone overlaying the capillary fringe of phreatic systems in the numerical analysis of our experiments.

We consider steady state transport of a conservative compound, described by the steady state version of the well-known advection-dispersion equation:

$$\mathbf{v} \cdot \nabla c - \nabla \cdot (\mathbf{D} \nabla c) = 0 \tag{2}$$

where c [$M\ L^{-3}$] is the concentration, $\mathbf{v} = \mathbf{q}/\theta$ [$L\ T^{-1}$] is the seepage velocity, θ is the volumetric water content equaling the effective porosity under water-saturated conditions, and $\mathbf{D}$ [$L^2\ T^{-1}$] is the dispersion tensor:

$$\mathbf{D} = \frac{\mathbf{v} \otimes \mathbf{v}}{\mathbf{v} \cdot \mathbf{v}} (D_\ell - D_t) + \mathbf{I} D_t \tag{3}$$

where $\mathbf{v} \otimes \mathbf{v}$ and $\mathbf{v} \cdot \mathbf{v}$ denote the tensor and scalar products of $\mathbf{v}$ with itself, respectively, and $\mathbf{I}$ is the identity matrix. D_ℓ [$L^2\ T^{-1}$] and D_t [$L^2\ T^{-1}$] are the longitudinal and transverse dispersion coefficients, respectively.

The experimental setup used in this work considers a continuous release of the solutes in the flow-through system under steady state conditions. In this case, dispersion occurs mainly in the directions perpendicular to the main flow, because from a sufficient distance to the source dispersive fluxes in the longitudinal direction can be neglected due to the small longitudinal concentration gradients compared to the ones in the transient direction [e.g., *Wexler*, 1992; *Zarlenga and Fiori*, 2013]. We further assume that the transverse dispersion coefficient D_t [$L^2\ T^{-1}$] is identical in both transverse directions.

Numerical and experimental studies have shown that incomplete mixing in pore channels arises during solute transport [e.g., *Chiogna and Bellin*, 2013; *Klenk and Grathwohl*, 2002; *Rolle et al.*, 2012; *Tartakovsky et al.*, 2009; *Willingham et al.*, 2008], especially under advection-dominated conditions. This results in a nonlinear dependence of transverse dispersion on the seepage velocity. In this study, we use an empirical parameterization of transverse dispersion [e.g., *Chiogna et al.*, 2010; *Rolle et al.*, 2012; *Ye et al.*, 2015] based on an earlier statistical model [i.e., *Bear and Bachmat*, 1967]:

$$D_t = D_p + D_{aq} \left(\frac{Pe^2}{Pe + 2 + 4\delta^2} \right)^{\beta} \tag{4}$$

where $Pe = vd/D_{aq}$ is the grain Péclet number, v [$L\ T^{-1}$] is the absolute value of the seepage-velocity vector, d [L] is the average grain size, δ is the ratio between the length of a pore channel and its hydraulic radius, and β is an empirical exponent that accounts for the degree of incomplete mixing within the pore channels.

The mechanical-dispersion term of equation (4) entails a dependence on the aqueous diffusion coefficient of the transported solute. Previous studies [e.g., *Chiogna et al*., 2010; *Rolle et al*., 2012; *Ye et al*., 2015] have shown a good agreement between equation (4) and experimental results in homogeneous porous media, providing also an average estimate of the two parameters (i.e., $\beta = 0.5$ and $\delta = 5.37$) for a range of grain sizes between 0.2 and 1.5 mm.

2.2. Quantification of Transverse Mixing

Quantifying transverse mixing processes in heterogeneous porous media can be a challenging task since it is important to separate the purely advective effects of plume meandering, squeezing, and stretching from actual dilution, which ultimately is caused by diffusion [e.g., *Cirpka et al*., 2011; *Rahman et al*., 2005; *Rolle et al*., 2009]. In this section, we describe two metrics of transverse mixing in domains affected by high-permeability inclusions: the mixing-enhancement factor [*Werth et al*., 2006] and the flux-related dilution index [*Rolle et al*., 2009].

Figure 1 schematically shows the effect of a high-permeability inclusion on the flow field in an otherwise homogeneous 3-D confined water-saturated domain. Since the hydraulic conductivity of the inclusion, K_i [$L\ T^{-1}$], is larger than the hydraulic conductivity of the matrix, K_m [$L\ T^{-1}$], streamlines are focused in the inclusion, as shown by the black lines in Figure 1. In the inclusion, the flow velocity is higher than in the surrounding matrix, which has three effects: (1) the transverse dispersion coefficient D_t is higher in the inclusion than outside, (2) the time for a water parcel to pass the inclusion is smaller than the time needed to travel the same distance in the matrix, and (3) the vertical and horizontal distances between streamlines are smaller in the inclusion than outside so that a transverse dispersive mass exchange between two streamlines has to cover a smaller distance inside the inclusion than outside. An additional effect of the inclusion is that its larger grain size increases not only the hydraulic conductivity but also the transverse hydrodynamic dispersion coefficient; such increase of D_t is beyond the velocity-related effect listed above.

2.2.1. Mixing-Enhancement Factor

Werth et al. [2006] introduced the mixing-enhancement factor to quantify the enhancement of transverse mixing by a rectangular high-permeability inclusion of length L_i [L] and height h_i [L], inserted in a homogeneous two-dimensional matrix of length L_{tot} [L] and height h_{tot} [L].

Considering the characteristic dispersion length δ [L], which is commonly defined as $\delta = \sqrt{2Dt}$ (where t [T] is the time available for mixing and D [$L^2\ T^{-1}$] represents the hydrodynamic dispersion coefficient), *Werth et al*. [2006] assumed two limiting situations under steady state flow conditions.

In the first case, the entire flow is focused in the high-permeability inclusion *i*. The degree of mixing in the vertical direction is expressed by the dimensionless ratio defined as

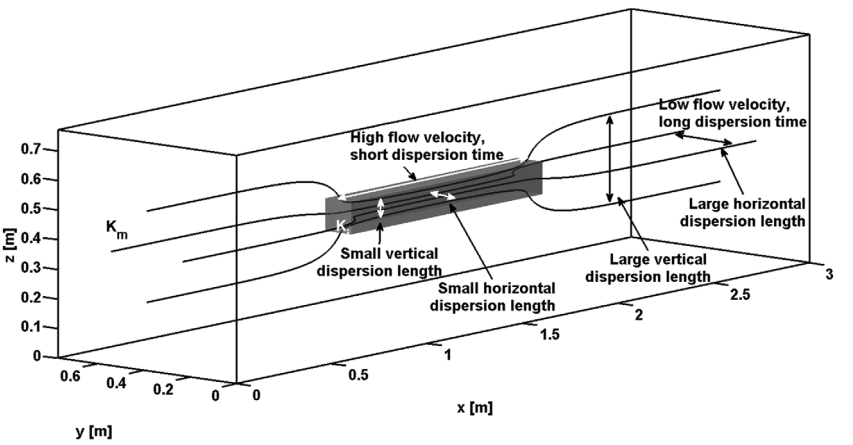

Figure 1. Schematic overview of flow focusing effects in a high-permeability inclusion in a 3-D flow-through system. Gray volume: high-permeability inclusion; black lines: streamlines.

$$\frac{\delta_{tv,i}}{h_i} = \frac{1}{h_i}\sqrt{\frac{2D_{t,i}L_i}{v_i}} \tag{5}$$

where $\delta_{tv,i}$ [L] is the characteristic dispersion length in the vertical direction, $D_{t,i}$ [$L^2\ T^{-1}$] denotes the transverse dispersion coefficient in the inclusion, and the time t is substituted by the ratio between the length of the inclusion and the seepage velocity in the inclusion v_i [$L\ T^{-1}$].

In the second case, the inclusion is not present and the medium is homogeneous. Hence, the degree of mixing reads as

$$\frac{\delta_{tv,m}}{h_{tot}} = \frac{1}{h_{tot}}\sqrt{\frac{2D_{t,m}L_i}{v_m}} \tag{6}$$

where $\delta_{tv,m}$ [L] is the characteristic dispersion distance in the vertical direction within the homogeneous matrix, $D_{t,m}$ [$L^2\ T^{-1}$] denotes the transverse vertical dispersion coefficient in the homogeneous matrix, and v_m [$L\ T^{-1}$] is the seepage velocity in the homogeneous matrix.

The mixing-enhancement factor for two-dimensional domains is then defined as the ratio of expressions in equations (5) and (6):

$$MF_{i,v} = \frac{h_{tot}}{h_i}\sqrt{\frac{D_{t,i}v_m}{D_{t,m}v_i}} \tag{7}$$

Assuming that the total discharge Q_{tot} [$L^3\ T^{-1}$] passes through the inclusion and considering the conservation of flow in the domain we can express v_i as

$$Q_{tot} = \theta_i v_i h_i = \theta_m v_m h_{tot} \Rightarrow v_i = \frac{v_m \theta_m h_{tot}}{\theta_i h_i} \tag{8}$$

where θ_i and θ_m are the effective porosities in the inclusion and in the homogeneous matrix, which are assumed identical for simplicity.

Under these idealized assumptions, the mixing-enhancement factor for a two-dimensional system reads as

$$MF_{i,v} = \sqrt{\frac{D_{t,i}h_{tot}}{D_{t,m}h_i}} \tag{9}$$

Note that two-dimensional transverse mixing is enhanced even for the unrealistic case that the transverse dispersion coefficients are identical within the inclusion and in the matrix, $D_{t,i} = D_{t,m}$. *Werth et al.* [2006] also considered the less idealized case in which not the entire discharge passes through the inclusion. In this case, transverse mixing outside the inclusion is reduced, but the average effect over the entire domain width was still an increase even for $D_{t,i} = D_{t,m}$.

We now consider the effect of a single high-permeability inclusion in a 3-D domain. Similarly to the 2-D case, we can define vertical ($MF_{i,v}$) and horizontal ($MF_{i,h}$) mixing-enhancement factors for a three-dimensional domain, of length L_{tot} [L], height h_{tot} [L], and width w_{tot} [L], for an inclusion of length L_i [L], height h_i [L], and width w_i [L]:

$$MF_{i,v} = \frac{h_{tot}}{h_i}\sqrt{\frac{D_{t,i}v_m}{D_{t,m}v_i}} \tag{10}$$

$$MF_{i,h} = \frac{w_{tot}}{w_i}\sqrt{\frac{D_{t,i}v_m}{D_{t,m}v_i}} \tag{11}$$

In the three-dimensional case, the total discharge is defined as

$$Q_{tot} = \theta_i v_i h_i w_i = \theta_m v_m h_{tot} w_{tot} \Rightarrow v_i = \frac{v_m \theta_m h_{tot} w_{tot}}{\theta_i h_i w_i} \tag{12}$$

such that equations (10) and (11), assuming a constant porosity, become

$$MF_{i,v} = \sqrt{\frac{D_{t,i} h_{tot} w_i}{D_{t,m} h_i w_{tot}}} \tag{13}$$

$$MF_{i,h} = \sqrt{\frac{D_{t,i} w_{tot} h_i}{D_{t,m} w_i h_{tot}}} \tag{14}$$

These expressions show that mixing enhancement in three-dimensional domains is different than in two dimensions. For illustration, we may consider the enhancement of vertical mixing by a high-permeability inclusion. Equation (13) differs from equation (9) by the factor $\sqrt{w_i/w_{tot}}$, where w_i is the width of the inclusion and w_{tot} that of the domain. Note that $w_i \leq w_{tot}$, implying that the three-dimensional mixing-enhancement factor is smaller than the two-dimensional one. For the specific case of isotropic flow focusing, i.e., $w_i/w_{tot} = h_i/h_{tot}$, the geometric effects of mixing enhancement in equations (13) and (14) cancel, and the only remaining enhancement is caused by transverse dispersion within the inclusion being larger than outside, $D_{t,i} > D_{t,m}$.

We have tested the proposed relations for 3-D mixing enhancement by performing numerical transport simulations in a confined setup (length = 3 m, width = 0.77 m, and height = 0.77 m) with a high-permeability inclusion (Figure 1). The inclusion width was changed in different simulations, whereas its length and height were fixed and equal to 0.2 and 0.066 m, respectively. The permeability ratio between the inclusion and the matrix was 13 and the mean hydraulic gradient was set to 1.84×10^{-3}. Both the width and the height of the plume source were 0.0462 m. As shown in Figure 2a, an increase in the width of the inclusion enhances mixing in the vertical direction ($MF_{i,v}$) since it leads to a longer residence time of the plume in the inclusion (the velocity v_i is reduced). On the contrary, if we consider the horizontal mixing-enhancement factor $MF_{i,h}$ (Figure 2a), we can observe a reduction in the mixing enhancement since, as w_i increases, the flow is distributed over a larger width. Considering the same model setup (i.e., variable inclusion width, constant length, and height), we measure the square root of the second central moment of the plume at the outlet of the domain in both directions, $\sqrt{M_{2C,v}}$ [L] and $\sqrt{M_{2C,h}}$ [L], defined as

$$\sqrt{M_{2C,v}} = \sqrt{\frac{\int_0^{h_{tot}} (z - M_{1,v})^2 c_v dz}{\int_0^{h_{tot}} c_v dz}} \tag{15}$$

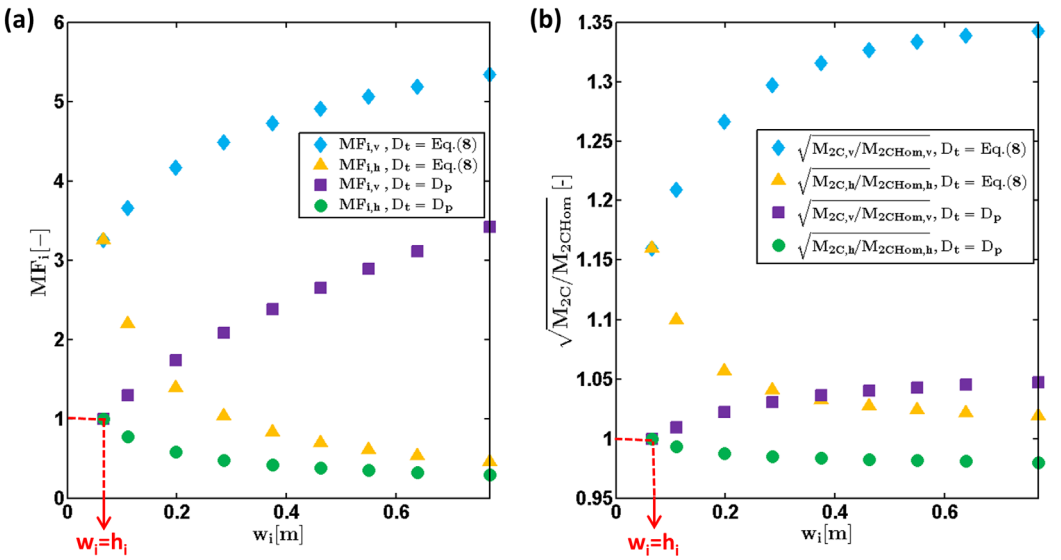

Figure 2. Metrics of transverse mixing enhancement by a high-permeability inclusion in a 3-D model domain as function of the inclusion width. (a) Mixing-enhancement factor; (b) square root of the normalized second central moment. Blue diamonds: metrics of vertical transverse mixing enhancement with D_t according to equation (4); yellow triangles: metrics of horizontal transverse mixing enhancement with D_t according to equation (4); purple squares: metrics of vertical transverse mixing enhancement with pure pore diffusion $D_p = 1.92 \times 10^{-10}$ m^2/s; green circles: metrics of horizontal transverse mixing enhancement with pure pore diffusion $D_p = 1.92 \times 10^{-10}$ m^2/s. Red dashed line: symmetric case ($w_i = h_i$ and $w_{tot} = h_{tot}$).

$$\sqrt{M_{2C,h}} = \sqrt{\frac{\int_0^{w_{tot}} (y - M_{1,h})^2 c_h dy}{\int_0^{w_{tot}} c_h dy}} \tag{16}$$

where $M_{1,v}$ [L] and $M_{1,h}$ [L] are the first spatial moment in vertical and horizontal directions, defined as

$$M_{1,v} = \frac{\int_0^{h_{tot}} z c_v dz}{\int_0^{h_{tot}} c_v dz} \tag{17}$$

$$M_{1,h} = \frac{\int_0^{w_{tot}} y c_h dy}{\int_0^{w_{tot}} c_h dy} \tag{18}$$

and c_v and c_h represent the average concentration of c_{norm} along horizontal and vertical directions, respectively:

$$c_v = \frac{\int_0^{w_{tot}} c_{norm} dy}{w_{tot}} \tag{19}$$

$$c_h = \frac{\int_0^{h_{tot}} c_{norm} dz}{h_{tot}} \tag{20}$$

In Figure 2b, we normalize $\sqrt{M_{2C,v}}$ and $\sqrt{M_{2C,h}}$ by the square root of the second central moment computed for the homogeneous porous medium (i.e., same setup but without the inclusion): $\sqrt{M_{2C,v}/M_{2CHom,v}}$ and $\sqrt{M_{2C,h}/M_{2CHom,h}}$. Comparing Figures 2a and 2b, it can be observed that the two metrics show a remarkable qualitative agreement.

As shown in Figure 2, both vertical and horizontal mixing enhancement are significantly larger considering the velocity and grain-size-dependent parameterization of D_t by equation (4), in comparison to the mixing enhancement considering pure pore diffusion ($D_t = D_p$). In fact, the first model results in a spatially variable D_t that depends nonlinearly on the spatially variable flow velocity and grain size in the heterogeneous domain; whereas the second model assumes a constant and velocity-independent D_t. This result is already indicative of the relevance of the physical model used to parameterize transverse dispersion for the correct computation of mixing enhancement in heterogeneous porous media.

The red dashed line in Figure 2 refers to the case of isotropic flow focusing (i.e., $w_i/w_{tot} = h_i/h_{tot}$) with constant local dispersion coefficient (e.g., $D_t = D_p$). As analytically derived above, the mixing enhancement in both the vertical and the horizontal directions reduces to the ratio of the transverse dispersion coefficient in the inclusion over that in the matrix when flow focusing is identical in the horizontal and vertical directions. Therefore, if the dispersion coefficient did not depend on the flow velocity, no mixing enhancement would occur, independently of the magnitude of the dispersion coefficient (i.e., this effect cannot be avoided by using an effective dispersion coefficient, which is constant in the entire domain).

Figure 2 also demonstrates that anisotropic flow focusing, that is $w_i/w_{tot} \neq h_i/h_{tot}$ leads to a strong directional dependence of transverse mixing. The scenarios reported in the figure show a considerably larger enhancement in the transverse vertical direction. For the case with constant local dispersion coefficient (e.g., $D_t = D_p$), even a reduction of transverse mixing is possible (e.g., horizontal transverse mixing in Figure 2). In this case, the reduction of mixing time in the inclusion has a stronger effect on transverse mixing than the reduction of the corresponding transverse mixing length. At the same time, mixing in the other transverse direction is more strongly enhanced.

As shown above, studies based on two-dimensional simulations likely overestimate mixing enhancement by flow focusing compared to fully 3-D descriptions. On the contrary, modeling studies assuming a constant dispersion coefficient in heterogeneous porous media result in the underestimation of mixing enhancement.

2.2.2. Flux-Related Dilution Index and Reactor Ratio

Rolle et al. [2009] introduced the flux-related dilution index to quantify dilution of solute plumes by transverse mixing at steady state. This metric is a modification of the volume-related dilution index [*Kitanidis*, 1994], which defines dilution as a measure of the disorder in the spatial distribution of solute concentration and is equivalent to the exponential of the Shannon entropy. While the dilution index describes how a

solute slug is diluted in a volume, the flux-related dilution index represents a volumetric discharge and quantifies how a given solute mass flux is distributed over a larger water flux [e.g., *Chiogna et al.*, 2011a, 2012; *Rolle et al.*, 2009]. The flux-related dilution index $E_Q(x)$ [$L^3\ T^{-1}$] in a bounded domain is defined as

$$E_Q(x) = \exp\left[-\int_\Omega p_Q(x,y,z)\ln p_Q(x,y,z)q_x(x,y,z)dA\right] \tag{21}$$

where Ω is the cross section perpendicular to the water flux, $q_x(x,y,z)$ [$L\ T^{-1}$] is the specific-discharge component in the longitudinal direction x and $p_Q(x,y,z)$ is the flux-weighted probability density function of the transverse particle location defined as

$$p_Q(x,y,z) = \frac{c(x,y,z)}{\int_\Omega c(x,y,z)q_x(x,y,z)dA} \tag{22}$$

The normalized form of flux-related dilution index, denoted as reactor ratio $M_Q(x)$, is obtained by dividing equation (21) with the total flow rate Q_x [$L^3\ T^{-1}$]:

$$M_Q(x) = \frac{E_Q(x)}{Q_x} \tag{23}$$

The flux-related reactor ratio $M_Q(x)$ reaches its maximum value, $M_Q(x) = 1$, when the solute flux is uniformly distributed over the total water flux.

3. Experimental Setup

Multitracer experiments were conducted in a three-dimensional and in a quasi two-dimensional flow-through chamber. The 3-D flow-through system (Figure 3a) has inner dimensions of 30 cm × 7.7 cm × 10 cm (length × width × height), while the quasi 2-D domain has inner dimensions of 28 cm × 1.1 cm × 14 cm. Both flow-through chambers are made of acrylic-glass. The 3-D setup is equipped with an array of 5 × 5 = 25 injection ports at the inlet and 7 × 7 = 49 extraction ports at the outlet. The ports at the inlet are equally spaced with a distance of 1.54 cm, while the distance at the outlet is 1.1 cm. The quasi 2-D flow-through chamber is equipped with seven injection ports at the inlet and seven extraction ports at the outlet, and the distance between each neighboring ports is 1.27 cm. All ports were connected to high-precision peristaltic pumps (IPC-N, Ismatec, Glattbrugg, Switzerland). A fully water-saturated zone was kept at the height of 7.7 cm for the 3-D setup and 9 cm for the 2-D setup. Both systems had a phreatic groundwater surface overlain by a shallow capillary fringe and an unsaturated zone even though active pumping was restricted to the water-saturated zone. Fluran pump tubings (ID 0.64 mm, Ismatec, Glattbrugg, Switzerland) and stainless steel capillaries were used as connection materials. More details about the experimental setups have been provided by *Ye et al.* [2015]. The flow-through experiments were performed in a room with constant temperature (T = 22°C) at the average flow velocities of 1 and 5 m/d.

High-permeability inclusions of coarse glass-bead packings with hydraulic conductivity $K = 3.24 \times 10^{-2}$ m/s were inserted in a homogeneous matrix of hydraulic conductivity $K = 2.5 \times 10^{-3}$ m/s. These values of hydraulic conductivity were computed based on the grain sizes and on the empirical correlation proposed by *Hazen* [1892], i.e., $K = (C \cdot d)^2$, where $C = 100\ \mathrm{m}^{-0.5}\ \mathrm{s}^{-0.5}$ and d [L] is the grain size. We constructed three heterogeneous setups for the 3-D flow-through system (Figure 3b) and one heterogeneous setup for the 2-D flow-through chamber. We used a grain size of 0.4–0.6 mm for the low-permeability matrix and a larger grain size of 1.6–2.0 mm for the high-permeability inclusions (Sigmund Lindner, Warmensteinach, Germany). In the experiments performed in the quasi 2-D porous medium, we inserted a single high-permeability inclusion. The size of the inclusion was 9 cm × 1.1 cm × 1.2 cm. The center of the lens was located 14 cm downstream of the inlet and 4.5 cm above the bottom of the 2-D flow-through chamber.

The front and side views of the three heterogeneous setups for the 3-D flow-through system and the dimensions and locations of the inclusions are shown in Figure 3b. One, two, and three inclusions were inserted in the homogeneous porous matrix to obtain three different flow configurations. The three cases are named Case 1, Case 2, and Case 3, respectively. The total volume of high-permeability material, as well as the ending position of the inclusions along the flow direction, was kept the same in the three

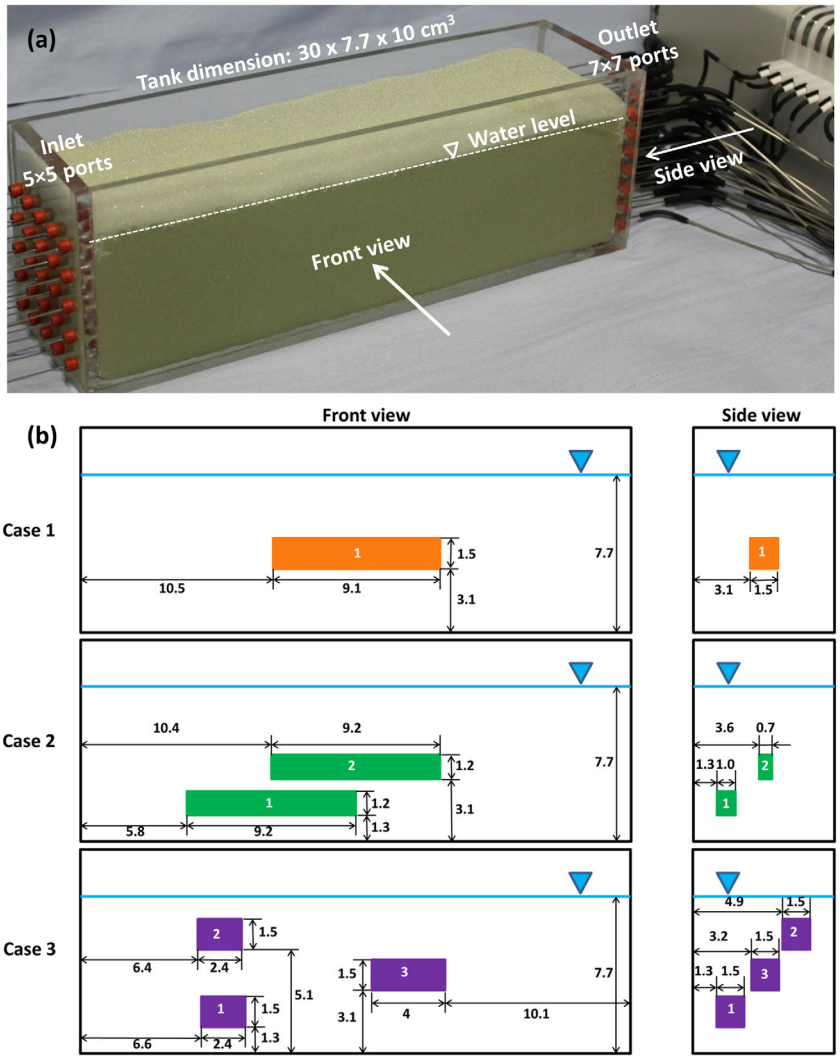

Figure 3. (a) Photograph of the 3-D flow-through chamber; (b) front and side view of the 3-D heterogeneous setups: black rectangles represent the flow-through chamber, blue lines denote the water level, orange, green, and purple rectangles represent the high-permeability inclusions for Case 1, Case 2, and Case 3, respectively.

heterogeneous setups. We always filled the material into the domains under water-saturated conditions to prevent air entrapment in the porous media [*Haberer et al.*, 2012]. The measured total porosity was 0.4 for both the matrix and the high-permeability inclusions.

Two tracers, namely fluorescein and oxygen, were simultaneously transported in the flow-through system. The two tracers have significantly different aqueous diffusion coefficients, namely 4.8×10^{-10} m^2/s for fluorescein and 1.97×10^{-9} m^2/s for oxygen at T = 22°C [e.g., *Atkins*, 1990; *Worch*, 1993]. After reaching steady state flow conditions, an oxygen-depleted sodium fluorescein solution was injected through the central port at the inlet, whereas an ambient solution with no fluorescein and oxygen concentration of 8.5 mg/L was continuously injected from the surrounding inlet ports. The tracer solution was kept in a gastight Tedlar bag (Alltech, Germany) to keep the oxygen concentration smaller than 1.0 mg/L. The fluorescein concentration in the tracer solution was 15 mg/L. After injection of three pore volumes, the plumes of fluorescein and oxygen had reached steady state. Samples were collected at the outlet ports twice for each experimental run, with a time interval of half a pore volume. The flow rate was experimentally determined by weighing the collected samples at each port, and the fluorescein concentration was measured using a UV-spectrometer (Perkin Elmer LS-3B). The oxygen concentration was measured using a noninvasive optode technique [see *Haberer et al.*, 2011 for details] at each of the 49 flow-through vials at the outlet and at the central flow-through vial at the inlet of the setup [*Ye et al.*, 2015]. The concentration and mass-flux values

were in excellent agreement between the two subsequent measurements and the results in the following are presented as the average of the two measurements.

4. Model Description and Validation

In order to interpret the experimental results, we performed flow and transport simulations using the numerical code recently presented by *Cirpka et al.* [2015] with slight modifications discussed below. The domain was discretized into 150 × 35 × 41 cells for the 3-D setup, with $\Delta x = 0.2$ cm and $\Delta y = \Delta z = 0.22$ cm. For the 2-D setup, the domain was discretized into 140 × 5 × 41 cells, with $\Delta x = 0.2$ cm, $\Delta y = 0.22$ cm, and $\Delta z = 0.254$ cm.

The governing flow equation was solved using a cell-centered Finite Volume method. The flow-through system was simulated as an unconfined medium, which is consistent with the experimental setup. Boundary conditions were set as constant flow at the inlet and at the outlet ports. No-flow boundary conditions were set to the bottom and the sides of the flow-through chamber. Since the flow-through systems were unconfined, unsaturated conditions were accounted for at the top of the domain, using the Mualem/van-Genuchten-parameterization [*van Genuchten*, 1980] and unsaturated parameters reflecting coarse sand [*Carsel and Parrish*, 1988]. This extension was necessary because a small fraction of the discharge passed through the overlaying unsaturated zone where the hydraulic conductivity was reduced but not zero [see also *Haberer et al.*, 2014]. The particle-tracking scheme of *Pollock* [1988] was used to compute streamlines.

Steady state advective-dispersive transport was simulated in *y-z* cross sections at regular distances in *x*. In each cross section, we used Voronoi tessellation to construct polygons centered about the points where the streamlines intersected with the observation plane. Then, transport from one cross section to the next could be simulated by a Finite Volume method for transverse dispersion, in which time is replaced by the individual plane-to-plane travel time along each streamline. In contrast to *Cirpka et al.* [2015], we imposed zero mass-flux boundary conditions at the bottom, side, and top boundaries, and a constant mass-flux boundary condition at the inlet face. The advantage of this numerical scheme is the significant reduction of numerical dispersion in comparison to numerical solutions which rely on fixed Cartesian grids. The parameters used in the numerical code are listed in Table 1.

To show the low numerical dispersion affecting the numerical scheme, we computed the ratio between the flux-related dilution index in a three-dimensional confined domain similar to the one shown in Figure 1 (i.e., length = 3 m, width = 0.77 m, height = 0.77 m). This domain has a horizontal upper boundary and is water saturated over the entire height, unlike the experimental device. The domain contains a high-permeability inclusion (length = 0.2 m, width = 0.066 m, height = 0.066 m) located at a distance of 1.8 m from the inlet and in the corresponding homogenous case. The ratio between the conductivity value in the high-permeability inclusion and in the surrounding matrix is 13. This permeability contrast causes the focusing of the plume in the inclusion. We imposed the conditions $h_i = w_i$ and $h_{tot} = w_{tot}$ and considered the case in which D_t is parameterized according to equation (4) and the case in which D_t is constant ($D_t = D_p = 1.92 \times 10^{-10}$ m^2/s). Figure 4 shows that in the first case transverse mixing is enhanced due to the difference in the dispersion coefficients, while in the second case the high-permeability inclusion does not cause an increase of the flux-related dilution index. As discussed in section 2.2.1, the latter behavior is expected for the case of pure pore diffusion. The fact that the numerical scheme reproduces this behavior indicates that the method is free of significant numerical transverse dispersion.

Table 1. Summary of Flow and Transport Parameters Used in the Model

Parameter	Value
Average fine grain diameter (mm)	0.5
Average coarse grain diameter (mm)	1.8
Porosity fine material	0.4
Porosity coarse material	0.4
Hydraulic conductivity fine material (m/s)	2.5×10^{-3}
Hydraulic conductivity coarse material (m/s)	3.24×10^{-2}
Van Genuchten parameter α[a] (m^{-1})	7.9
Van Genuchten parameter N[a]	35.8
Aqueous diffusion coefficient fluorescein[b] (m^2/s)	0.48×10^{-9}
Aqueous diffusion coefficient oxygen[b] (m^2/s)	1.97×10^{-9}
Parameter δ of D_t (equation (4))[c]	5.37
Parameter β of D_t (equation (4))[c]	0.5

[a]From *Haberer et al.* [2011], consistent with *McCray and Falta* [1997].
[b]From *Worch* [1993] and *Atkins* [1990], at $T = 22$°C.
[c]From *Ye et al.* [2015].

5. Results and Discussion

The numerical model described in the previous section was used to interpret the

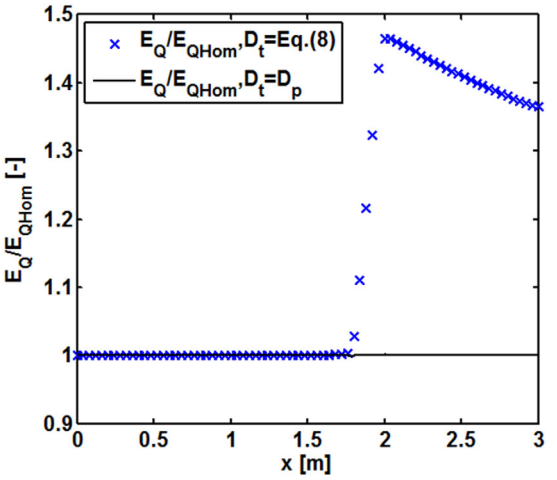

Figure 4. Validation of the numerical scheme in a 3-D scenario with ratio of flux-related dilution index between heterogeneous and homogeneous cases along the travel distance. Blue crosses: simulations with D_t according to equation (4); black line: simulations with $D_t = D_p$ (pure pore diffusion).

experimental data and to quantitatively illustrate the effects of flow focusing on dilution and dilution enhancement observed in the flow-through experiments.

5.1. Effects of Flow Focusing in 3-D Heterogeneous Setups

Figure 5a shows the simulated influence of the high-permeability inclusions on the flow field for the three-dimensional setups. Streamlines were traced from the injection port to the end of the flow-through system. As can be observed, they converge towards the high-permeability inclusions. However, due to the nonuniformity of the flow field, some streamlines diverge from the initial bundle. In Case 1, all streamlines are focused at a distance of $x = 0.1$ m and defocused at a distance of $x = 0.2$ m. The focusing zone of the streamlines is exactly the location where the high-

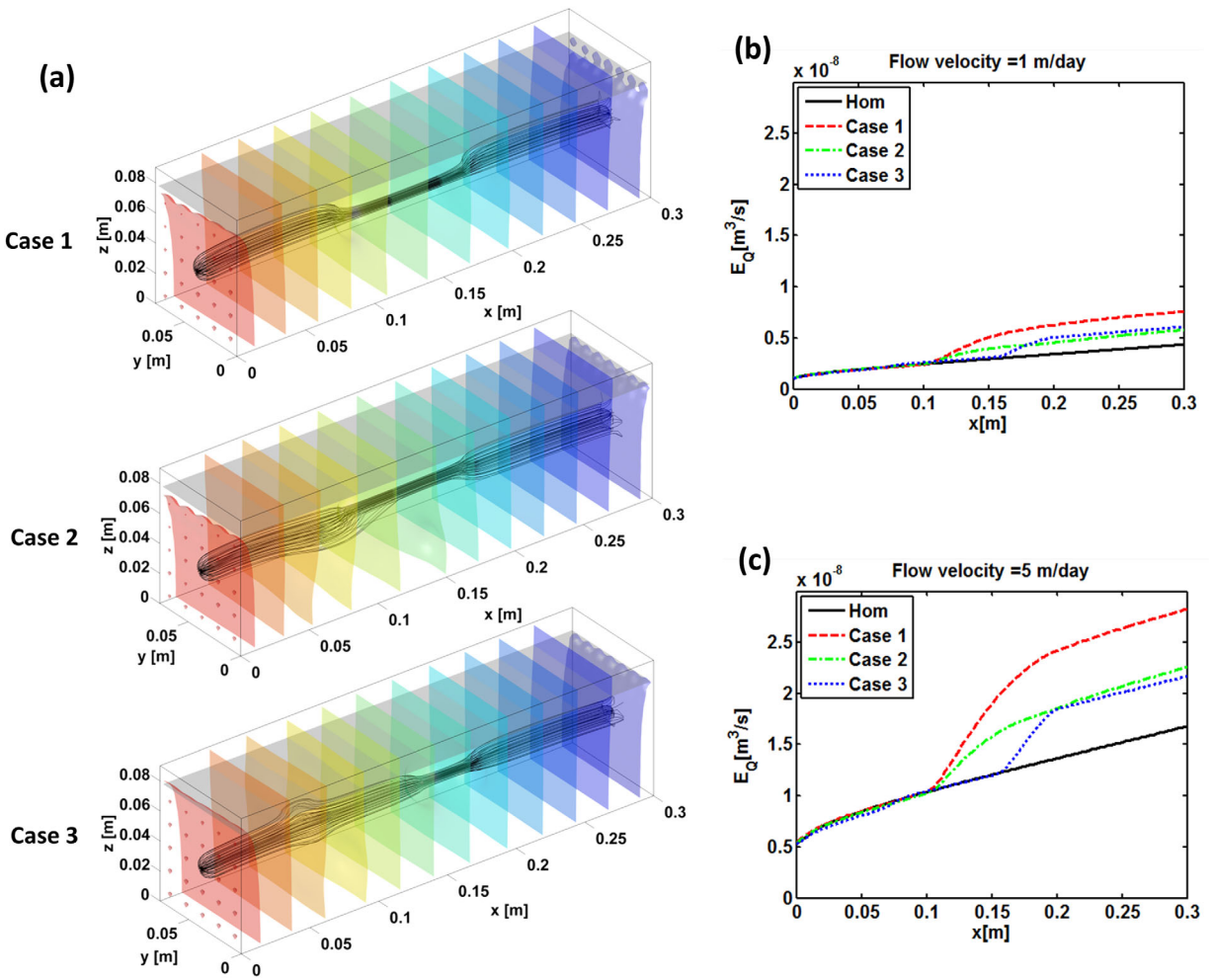

Figure 5. (a) Streamlines (black lines) starting from the central inlet port, isopotential surfaces (colored surfaces), and water level (gray surface). (b) Flux-related dilution index in the flow-through chambers for the three heterogeneous cases and the homogeneous case for a mean flow velocity of 1 m/d. (c) Flux-related dilution index in the flow-through chambers for the three heterogeneous cases and the homogeneous one for a mean flow velocity of 5 m/d.

permeability inclusion lies (see Figure 3). The focusing of flow reduces the distance between streamlines, increases concentration gradients transverse to the flow direction, but reduces the mixing time within the inclusion. While the geometric effects should cancel for the given geometry (see the discussion on isotropic flow focusing above), the higher velocity within the inclusion causes an increased local transverse dispersion coefficient, the effect of which prevails in enhanced dilution, as reflected by the flux-related dilution index in Figures 5b and 5c. At the two flow velocities of 1 and 5 m/d, the red dashed line shows a jump in the flux-related dilution index (E_Q), with a higher slope, after a travel distance of $x = 0.1$ m; E_Q returns to the initial rate of increase after a travel distance of $x = 0.2$ m (i.e., after the high-permeability inclusion).

In Case 2, a few streamlines deviate from the flow path at a distance of $x = 0.06$ m. This happens at the position where the first high-permeability inclusion is located (see Figure 3). For the given asymmetric setup, the plume fringe is not completely focused within the inclusion. Outside the inclusion, the streamlines meander in zones with lower-than-the-average flow velocity. As a consequence, while transverse mixing is enhanced within the inclusion, it is reduced in the fraction of the plume outside the high-conductivity material. The net effect is that the presence of the first inclusion does not enhance dilution (Figures 5b and 5c, green dash-dotted lines). When the plume reaches the second lens at the travel distance of $x = 0.1$ m, all streamlines injected at the source are focused. Like in Case 1, dilution is stronger in the inclusion due to the higher velocity causing the enhancement of transverse mass exchange. This is illustrated by the increasing slope of the flux-related dilution index starting at a travel distance of $x = 0.1$ m (Figures 5b and 5c). The rate of dilution enhancement along the travel distance is smaller for Case 2 compared to Case 1. This is due to the stronger flow focusing effect in the larger cross-sectional area of the inclusion in Case 1 (2.25×10^{-4} m^2) than in Case 2 (0.84×10^{-4} m^2).

Case 3 shows a different development of the streamlines than the other two cases. At a distance of $x = 0.06$ m, the streamlines deviate in both lateral and vertical directions due to the presence of two surrounding high-permeability inclusions (Figure 3). As shown by the blue dotted line in Figures 5b and 5c, the overall dilution in the first half of the domain is the same as for the homogeneous medium at the flow rate of 1 m/d whereas it is even smaller at the flow rate of 5 m/d. At the flow rate of 1 m/d, a balance occurs between dilution enhancement due to flow focusing inside the inclusions and the dilution decrease in the low velocity zones outside the lenses. At a higher flow rate, fewer streamlines carrying nonzero concentration are focused in the high-permeability inclusions. Hence, the decrease of dilution becomes slightly larger than the dilution enhancement. The third high-permeability inclusion appearing at a distance of $x = 0.15$ m focuses the flow as in Case 1. However, since the inclusion is shorter compared to Case 1, lower dilution values are reached at the end of the domain.

For both flow velocities (1 and 5 m/d), the observed behavior is qualitatively the same, but the values of the flux-related dilution index are larger when the flow-through system is run at higher velocity. It should be

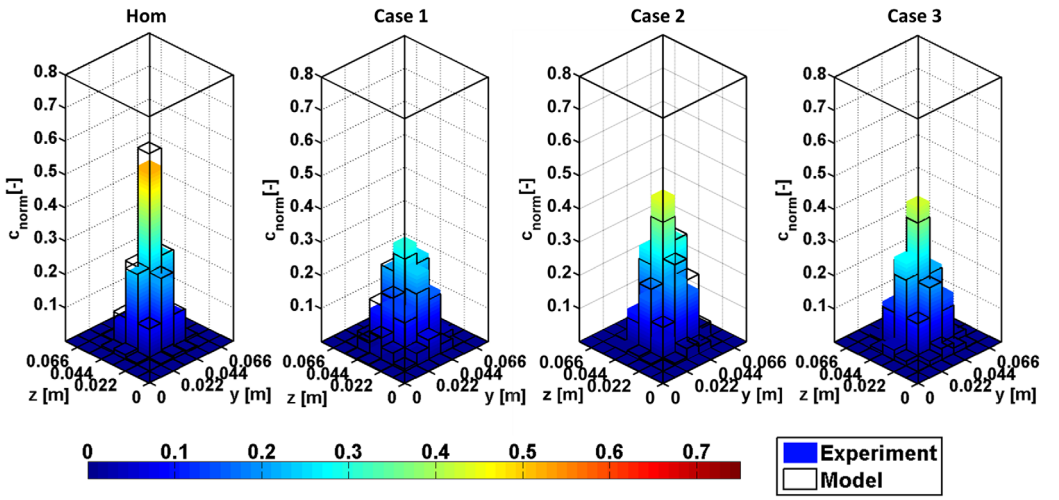

Figure 6. Normalized fluorescein concentration distributions at the outlet for the 3-D homogeneous setup and the three 3-D heterogeneous setups: observed and simulated values at flow velocity of 1 m/d.

noted, however, that the dimension of the flux-related dilution index is that of a discharge. In the cases with a mean velocity of 5 m/d, the discharge is 5 times larger than the one for the cases with 1 m/d. The values of the flux-related dilution index, however, are less than 5 times larger because the transverse dispersion coefficients increase less than linearly with the seepage velocity. That is, the reactor ratio, which scales the flux-related dilution index by the total discharge, is smaller in the case with higher mean flow velocity.

All heterogeneous setups enhance transverse mixing in comparison to the homogeneous setup. Case 1 shows the strongest dilution enhancement, whereas Case 2 has the lowest dilution enhancement at the flow velocity of 1 m/d and Case 3 has the lowest dilution enhancement at the flow velocity of 5 m/d. This difference in the behavior of the dilution enhancement can be explained by considering that the inclusions have different geometries and that the transverse dispersion coefficient depends nonlinearly on the flow velocity.

Normalized fluorescein concentrations at the outlet ports are shown in Figures 6 and 7, for the flow velocities of 1 m/d and 5 m/d, respectively. Results of the 3-D homogeneous setup investigated by *Ye et al.* [2015] are also included in the plots for a direct comparison with the heterogeneous cases that are the focus of the present study. Color columns denote experimental measurements at the 7 × 7 outlet ports, whereas black outlines represent the results of forward simulations carried out without any parameter fitting using the 3-D numerical model presented in section 4. The match between experimental measurements and model results is good for all cases at both flow rates. We evaluated the model performance according to the χ^2 test, defined as

$$\chi^2 = \frac{1}{n_{ports}} \sum_{n=1}^{n_{ports}} \frac{(c_{meas} - c_{simu})^2}{\varepsilon^2} \tag{24}$$

where n_{ports} is the number of ports (49 in our setup), c_{meas} is the measured normalized concentration at each port, c_{simu} is the simulated normalized concentration and ε is the experimental error, which we estimate a posteriori such that $\chi^2 \approx 1$. For the eight cases shown in Figures 6 and 7, the mean experimental error is always smaller than 11% and thus comparable to the values obtained in experiments with homogeneous porous media [*Ye et al.*, 2015].

As shown in Figure 6, the peak concentrations differ significantly among the four cases. The peak concentrations in the heterogeneous cases are smaller in comparison to the homogeneous case, due to dilution enhancement in the high-permeability inclusions. Furthermore, Case 1 shows the lowest peak concentration value, whereas Cases 2 and 3 have similar values. This is consistent with the dilution predicted by the numerical simulations and quantified by the flux-related dilution index (Figure 5). While the total volume of the high-permeability inclusions is practically the same in the three heterogeneous setups, different spatial distributions of the high-permeability material in the matrix cause different enhancement of transverse

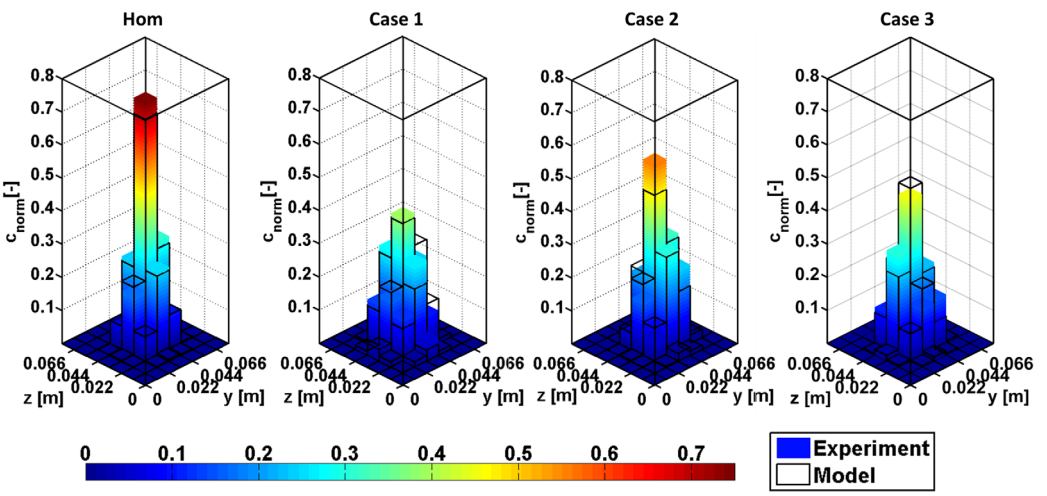

Figure 7. Normalized fluorescein concentration distributions at the outlet for the 3-D homogeneous setup and the three 3-D heterogeneous setups: observed and simulated values at flow velocity of 5 m/d.

mixing. Therefore, the volume ratio of the high-conductive to low-conductive materials and the conductivity contrast are not sufficient to predict plume dilution. In fact, the enhancement of transverse dispersion and dilution depends on how the plume fringe is focused in the high-permeability inclusions [e.g., *Chiogna et al*., 2011b; *de Barros et al*., 2012].

The results presented in Figure 7 for the high-velocity case are consistent with those presented in Figure 6. At higher flow velocity, the peak concentration is higher. This is due to the shorter residence time of the solute in the flow-through chamber in conjunction with a lower than linear dependence of transverse dispersion on the average flow velocity.

The flux-related dilution index and reactor ratio at the outlet of the domain have been computed for both experimental and model results at flow velocity of 1 and 5 m/d. They are listed in Table 2. The values of the flux-related dilution index, which have units of a discharge, are larger at 5 m/d than at 1 m/d. However, it should be noticed that at 5 m/d the total volumetric fluxes are also 5 times larger than the ones at 1 m/d. Thus, besides quantifying the absolute dilution of the plume with E_Q it is also useful to consider the degree of dilution for a given flow rate. To this end, the reactor ratio is a useful metric since it is normalized by the total discharge in the flow-through system. The reactor ratio is consistently higher for the experiments at lower flow velocity. As discussed above, this behavior is expected since at lower velocity the residence time is 5 times larger than at 5 m/d, whereas the local transverse dispersion coefficient is less than 5 times smaller.

The normalized error between the experimental dilution index $E_{Q,meas}$ and the model results $E_{Q,sim}$ (i.e., $\mathrm{abs}(E_{Q,meas} - E_{Q,sim})/E_{Q,sim}$) is within 10% except for Case 2. The larger error for Case 2 (20% at 1 m/d and 25% at 5 m/d) may be explained by the fact that the transition between high-conductivity and low-conductivity materials in the real experiment is not as sharp as assumed by the model. In fact, the small glass beads may intrude into the pore space of the large ones at the sides of the inclusions. The width of this transition zone has a dimension of 1–2 grains in our experimental setup. This effect can be neglected if the dimension of the inclusion is large, as in Cases 1 and 3, while in Case 2 the influence of this transition zone is more relevant, thus potentially explaining the larger difference between model and experimental results.

Besides considering the values of the flux-related dilution index and of the reactor ratio in the different setups, it is illustrative to consider the enhancement of dilution determined by flow focusing in the heterogeneous setups. Table 3 lists the enhancement of dilution with respect to the homogeneous case as the ratio between the flux-related dilution index at the outlet of the flow-through chamber in the heterogeneous cases and in the homogeneous case. The strongest dilution enhancement is observed for Case 1 (∼65%), whereas Cases 2 and 3 yield smaller enhancements. Furthermore, for a given setup, the dilution enhancement is similar for both velocities.

5.2. Effects of Dimensionality on Dilution and Dilution Enhancement

Dilution in three-dimensional domains is in general larger than in two-dimensions [*Kitanidis*, 1994], due to the additional degree of freedom provided by the third spatial dimension. This was confirmed in the experiments carried out in this study and substantiated by the values of the flux-related dilution index measured

Table 2. Experimental and Model Results of Flux-Related Dilution Index and Reactor Ratio at the Outlet of the 3-D Setups at Flow Velocity of 1 and 5 m/d

	1 m/d			5 m/d		
Setup	Experiment	Model	Norm. Error (%)	Experiment	Model	Norm. Error (%)
Flux-related dilution index (m^3/s)						
Hom	4.85×10^{-9}	5.13×10^{-9}	5	1.93×10^{-8}	2.10×10^{-8}	8
Case 1	7.83×10^{-9}	8.70×10^{-9}	10	3.16×10^{-8}	3.32×10^{-8}	5
Case 2	5.43×10^{-9}	6.78×10^{-9}	20	2.06×10^{-8}	2.73×10^{-8}	25
Case 3	6.20×10^{-9}	6.81×10^{-9}	9	2.46×10^{-8}	2.52×10^{-8}	3
Reactor ratio						
Hom	0.18	0.18	5	0.15	0.16	8
Case 1	0.28	0.31	10	0.23	0.24	5
Case 2	0.20	0.24	20	0.15	0.20	25
Case 3	0.23	0.25	9	0.19	0.19	3

Table 3. Ratio of Flux-Related Dilution Index at the Outlet of Flow-Through Chamber Between the 3-D Heterogeneous Porous Media and the 3-D Homogeneous Porous Medium (E_{QHet}/E_{QHom}) at Flow Velocity of 1 and 5 m/d

	1 m/d		5 m/d	
Heterogeneous Setup	Experiment	Model	Experiment	Model
Case 1	1.61	1.70	1.64	1.58
Case 2	1.12	1.32	1.07	1.30
Case 3	1.28	1.33	1.28	1.20

at the outlet of the flow-through setups (Tables 2 and 4). Despite high-permeability inclusions may considerably enhance dilution in both 2-D and 3-D systems, the mixing enhancement is different depending on the dimensionality of the domain (section 2.2.1). Indeed, the effect of high-permeability inclusions enhance dilution in a considerably different way in 2-D than in 3-D flow-through systems. To confirm this statement by experimental evidence, we compare the dilution enhancement between 2-D and 3-D cases, in a very simple setup. A single inclusion was inserted in the quasi 2-D flow-through chamber and the results were compared with the analogous setup in the 3-D flow-through chamber (Case 1). In both setups, the inclusions are centered, have the same length and a height equal to the interspacing between inlet ports thus allowing a meaningful comparison of the effects of dimensionality. Fluorescein was used as tracer and the experiments were run at mean flow velocities of 1 and 5 m/d.

Figure 8 shows the flux-related dilution index at the outlet of the flow-through chamber for both 2-D and 3-D experiments, considering both homogeneous and heterogeneous setups at the mean flow velocities of 1 and 5 m/d. Notice that to provide a meaningful comparison between 2-D and 3-D systems, the flux-related dilution index is normalized by subtracting its values at the inlet, which is significantly different between 2-D and 3-D setups. The difference between experimental (black bars) and model (white bars) results is smaller than 17% for all cases, showing the good performance of the model in predicting the experimental data. In both 2-D and 3-D setups, at a specific flow velocity, dilution is smaller in the homogeneous case than in the heterogeneous cases. Furthermore, the figure clearly illustrates that dilution is larger in the 3-D setup both in the homogeneous and in the heterogeneous porous media.

The absolute and normalized values of the flux-related dilution index as well as of the reactor ratio are listed in Table 4 for the 2-D and 3-D heterogeneous cases at flow velocity of 1 and 5 m/d. It is interesting to notice that, in contrast to the values of the flux-related dilution index, the reactor ratio shows larger values in the 2-D than in the 3-D system. This difference is due to the fact that the two metrics capture different features of plume dilution. Whereas the flux-related dilution index quantifies dilution that is larger in the 3-D cases, the reactor ratio expresses the degree of dilution and captures the fact that the solute mass flux is better distributed with respect to the total discharge in the 2-D than in the 3-D setups. The difference in the behavior of the flux-related dilution index and the reactor ratio is caused by the difference in the total discharge between 2-D and 3-D setups. Since the mean flow velocity is the same in both systems, the total discharge in the 3-D case is much larger than in the 2-D case. The reactor ratio is therefore indicative of the

Table 4. Experimental and Model Results of Flux-Related Dilution Index, Normalized Flux-Related Dilution Index, Reactor Ratio, and Normalized Reactor Ratio at the Outlet of the 2-D and the 3-D Heterogeneous Setups at Flow Velocity of 1 and 5 m/d

	3-D			2-D		
Flow Velocity	Experiment	Model	Norm. Error (%)	Experiment	Model	Norm. Error (%)
Flux-related dilution index (m^3/s)						
1 m/d	7.83×10^{-9}	8.70×10^{-9}	10	2.69×10^{-9}	2.95×10^{-9}	9
5 m/d	3.16×10^{-8}	3.32×10^{-8}	5	1.14×10^{-8}	1.30×10^{-8}	13
Normalized flux-related dilution index (m^3/s)						
1 m/d	6.71×10^{-9}	7.58×10^{-9}	12	2.05×10^{-9}	2.32×10^{-9}	11
5 m/d	2.61×10^{-8}	2.77×10^{-8}	6	8.21×10^{-9}	9.85×10^{-9}	17
Reactor ratio						
1 m/d	0.28	0.31	10	0.61	0.67	9
5 m/d	0.23	0.24	5	0.51	0.58	13
Normalized reactor ratio						
1 m/d	0.24	0.27	12	0.46	0.52	11
5 m/d	0.19	0.20	6	0.37	0.44	17

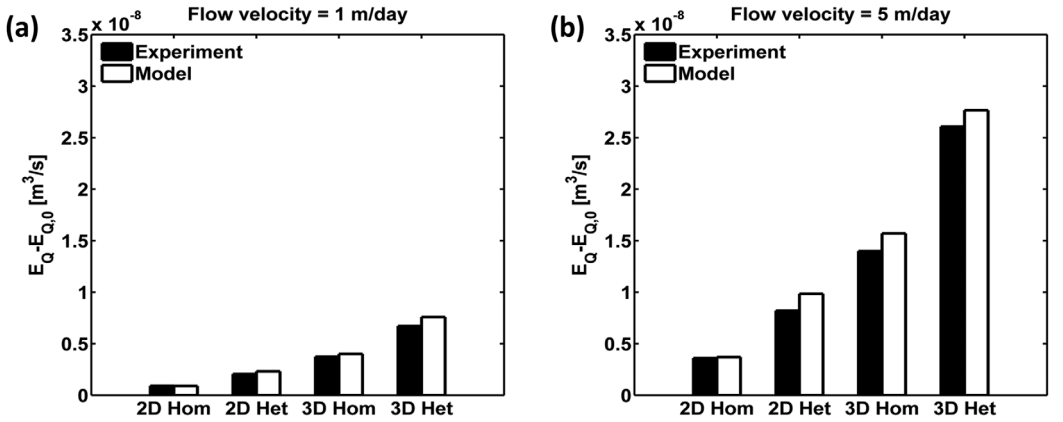

Figure 8. Experimental and model results of normalized flux-related dilution indices at the outlet of the flow-through chamber for four setups: 2-D homogeneous, 2-D heterogeneous, 3-D homogeneous, and 3-D heterogeneous at flow velocity of (a) 1 m/d and (b) 5 m/d.

potential for further dilution in the system: the larger the value at the outlet, the better the plume is diluted and the smaller is the potential for further dilution. Combining the information from the two metrics used to quantify the effects of transverse mixing on plume dilution, it is possible to conclude that in the 3-D setup the plume is certainly more diluted and also has a larger potential for further dilution than in the 2-D system.

As done in the previous analysis for the different 3-D cases, dilution enhancement is computed as the ratio of the flux-related dilution index between heterogeneous and homogeneous setups at the outlet of the flow-through system. The results are presented in Table 5. Although dilution is larger for the 3-D flow-through systems than for the 2-D ones, dilution enhancement is stronger for the 2-D heterogeneous system ($\sim$1.8) than for the 3-D heterogeneous setup ($\sim$1.6). This indicates that results obtained in 2-D systems may overestimate the enhancement of transverse mixing by flow focusing in comparison to fully 3-D domains.

To compare vertical and horizontal mixing enhancement in the three-dimensional setup with the mixing enhancement in the two-dimensional setup, we compute the mixing-enhancement factor (Table 6) according to equations (9), (13), and (14), respectively.

The dilution enhancement quantified in Table 5 ($\sim$1.6 for 3-D case and $\sim$1.8 for 2-D case) shows a qualitative agreement with the values based on the mixing-enhancement factor, reported in Table 6 ($\sim$3.0 for 3-D case and $\sim$6.5 for 2-D case). Both results show a lower mixing enhancement due to flow focusing in three-dimensional than in two-dimensional systems. Notice that equations (8) and (12) assume complete flow focusing in the high-permeability inclusions. Using numerical simulations, we verified that at both mean flow velocities the fringe of the plume is only partially focused in the inclusion. As suggested by *Werth et al*. [2006], some corrections can be applied in order to consider such effects and this would lead to smaller values of MF. However, it is noticeable that the analytical equations for MF, although only valid under simplifying assumptions, are qualitatively supported by the outcomes of the flow-through experiments and allow capturing the distinct mixing enhancement in 2-D and 3-D systems. Despite the simplicity of the geometry of the system, *Werth et al*. [2006] have shown that the main outcomes of their two-dimensional analysis performed in a simplified setup, is useful to qualitatively interpret more realistic heterogeneous field-scale results. Similarly, the modeling and experimental results presented in this contribution, quantitatively describe mixing processes at the local scale and can help interpreting field-scale processes. In particular,

Table 5. Ratio of the Flux-Related Dilution Index at the Outlet of Flow-Through Chamber Between Heterogeneous Porous Media and Homogeneous Porous Media for Both 3-D and 2-D Setups at Flow Velocity of 1 and 5 m/d

	3-D		2-D	
Flow Velocity	Experiment	Model	Experiment	Model
1 m/d	1.61	1.70	1.76	1.95
5 m/d	1.64	1.58	1.67	1.93

Table 6. Analytical Mixing-Enhancement Factor ($MF_{i,v}$ and $MF_{i,h}$ for 3-D and $MF_{i,v}$ for 2-D) at Flow Velocity of 1 and 5 m/d for 3-D and 2-D Heterogeneous Setups

	3-D		2-D
Flow Velocity	$MF_{i,v}$	$MF_{i,h}$	$MF_{i,v}$
1 m/d	3.2	3.2	6.9
5 m/d	2.8	2.8	6.2

they point to the relevance of considering fully three-dimensional structures in order to correctly describe mixing enhancement in porous media.

5.3. Compound-Specific Effects

In this part, we show the relevance of compound-specific effects upon transport of different solutes. Figure 9 shows the experimental and numerical results obtained at flow velocity of 5 m/d, using fluorescein (Figure 9a) and oxygen (Figure 9b) as tracer solutes. The normalized flux-related dilution index is reported for the 2-D and 3-D homogeneous and heterogeneous setups. Plume dilution at the outlet of the flow-through systems is larger for oxygen than for fluorescein in both 2-D and 3-D porous media. The match between the predictive model and the experimental results is satisfactory, although oxygen measurements are affected by a larger uncertainty than the fluorescein ones, as discussed by *Ye et al*. [2015].

Computed and simulated values for the flux-related dilution index and the reactor ratio are summarized in Table 7. The difference between the normalized flux-related dilution index and reactor ratio can be explained with the same arguments used in the previous sections: dilution is larger in 3-D than in 2-D, whereas the mass flux is better distributed with respect to the total discharge in the 2-D systems than in the 3-D setups.

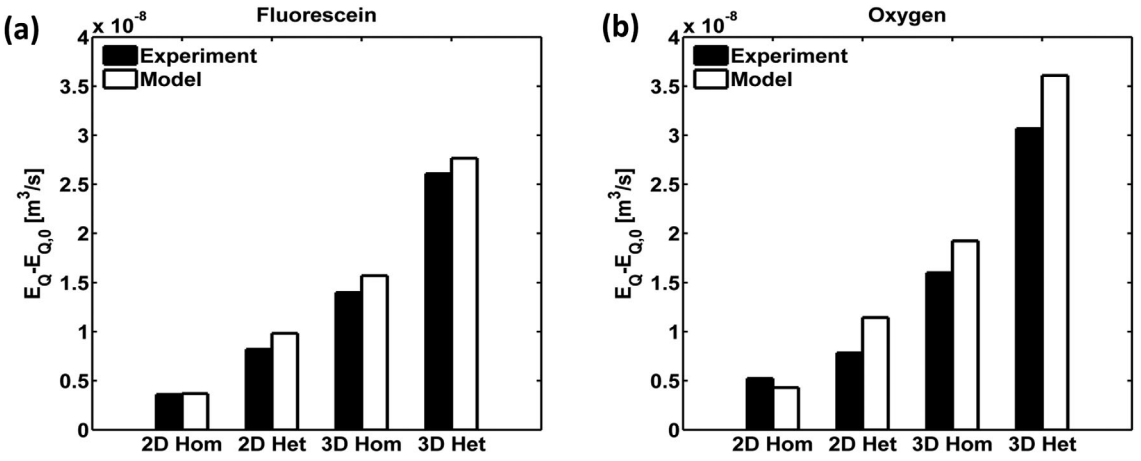

Figure 9. Experimental and model results of normalized flux-related dilution indices for (a) fluorescein and (b) oxygen tracer solutes at the outlet of the flow-through chamber for four setups: 2-D homogeneous, 2-D heterogeneous, 3-D homogeneous, and 3-D heterogeneous at flow velocity of 5 m/d.

Table 7. Experimental and Model Results of Flux-Related Dilution Index, Normalized Flux-Related Dilution Index, Reactor Ratio, and Normalized Reactor Ratio at the Outlet of the 2-D and the 3-D Heterogeneous Setups for Fluorescein and Oxygen Tracer Plumes at Mean Flow Velocity of 5 m/d

	3-D			2-D		
Solute	Experiment	Model	Norm. Error (%)	Experiment	Model	Norm. Error (%)
Flux-related dilution index (m^3/s)						
Fluorescein	3.16×10^{-8}	3.32×10^{-8}	5	1.14×10^{-8}	1.30×10^{-8}	13
Oxygen	3.62×10^{-8}	4.17×10^{-8}	13	1.10×10^{-8}	1.46×10^{-8}	25
Normalized flux-related dilution index (m^3/s)						
Fluorescein	2.61×10^{-8}	2.77×10^{-8}	6	8.21×10^{-9}	9.85×10^{-9}	17
Oxygen	3.07×10^{-8}	3.61×10^{-8}	15	7.84×10^{-9}	1.15×10^{-8}	32
Reactor ratio						
Fluorescein	0.23	0.24	5	0.51	0.58	13
Oxygen	0.26	0.30	13	0.49	0.66	25
Normalized reactor ratio						
Fluorescein	0.19	0.20	6	0.37	0.44	17
Oxygen	0.22	0.26	15	0.35	0.51	32

The experimental and modeling results shown in Figure 9 illustrate that compound-specific effects are not negligible even at very fast groundwater velocities (i.e., 5 m/d). In fact, also in such strongly advection-dominated regimes the transverse hydrodynamic dispersion coefficient and, in particular, the mechanical-dispersion term still depends on the diffusivity of the transported solutes, as also evidenced in previous theoretical and modeling works [e.g., *Bijeljic and Blunt*, 2007; *Scheven*, 2013]. This results in the larger dilution of oxygen plumes compared to the fluorescein plumes in the corresponding setups.

6. Conclusions

In this study, we theoretically analyzed, numerically simulated, and experimentally investigated dilution of steady state plumes in isotropic porous media with high-conductivity inclusions, with a simple geometry. We measured highly resolved concentration profiles and volumetric flow rates at the outlet of three different three-dimensional flow-through systems. The three different heterogeneous cases were obtained by inserting the same volume of high-permeability material into a homogeneous low-permeability matrix, but varying the geometry and the location of the inclusions. Dilution was quantified by the flux-related dilution index, which could be calculated for all travel distances in numerical simulations and at the outlet of the flow-through system in the experiments. The main outcomes of this study can be summarized as follows:

1. In high-permeability inclusions, both distances between streamlines and the time needed to travel a certain longitudinal distance are shortened. In 2-D systems, the effect of decreasing the transverse dispersion distance always prevails over the effect of decreasing the time available for mixing, thus resulting in an enhancement of transverse mixing and dilution in the inclusions even for the hypothetical case of pure, velocity-independent pore diffusion. In 3-D systems, the two effects cancel when flow focusing in the two transverse directions is identical. If flow focusing is anisotropic in the two transverse directions, the geometric effect is an increase in mixing in the direction in which the plume fringe is more strongly focused and a decrease in the direction corresponding to less focusing. In the simplified laboratory condition considered in this study, the mixing enhancement predicted for 2-D flow is the upper limit of that in 3-D media. The higher velocity in the high-conductivity inclusion, however, also leads to a higher value of the local transverse dispersion coefficient, which is further magnified by a larger grain size within the high-conductivity material. This effect leads to an enhancement of 3-D transverse mixing if the plume fringe lies within the high-permeability inclusion, regardless of the geometry.
2. When the plume fringe is not focused within the high-permeability inclusion, the plume meanders in regions with lower flow velocity and dilution by transverse mixing diminishes. Therefore, the total dilution depends not only on the extent of the permeability contrast between the coarse material and the matrix and on the volumetric ratio of the two materials, but also on the exact spatial arrangement of the inclusions with respect to the location of the plume fringes. In all three heterogeneous setups studied in the experiment, dilution is enhanced in comparison to the homogeneous flow-through system, but to different extents. These results are in agreement with observations performed in similar two-dimensional experimental [e.g., *Rolle et al*., 2009] and modeling studies [e.g., *Werth et al*., 2006; *Chiogna et al*., 2011a].
3. Plume dilution by transverse mixing is more pronounced in the 3-D flow-through systems than in the 2-D system because transverse dispersion acts in two transverse directions in the 3-D case and only in one direction in the 2-D case. However, the dilution enhancement by flow focusing in high-permeability inclusions is larger in the quasi 2-D flow-through setup. Furthermore, we have shown that assuming a constant dispersion coefficient, which is a common assumption in stochastic subsurface hydrology, may lead to a significant underestimation of transverse-mixing enhancement in three-dimensional flow fields. Hence, it is crucial to determine the dimensionality of the problem and to correctly parameterize local dispersion to accurately interpret and model mixing processes in porous media.
4. The diffusivity of the transported solute affects the transverse hydrodynamic dispersion coefficient not just at low but also at high flow velocities, both in 2-D and 3-D systems. The relative importance of the local transverse dispersion coefficient for the enhancement of plume dilution is larger in 3-D than in 2-D systems [*Ye et al*., 2015], so that compound-specific effects on plume dilution are also more pronounced in 3-D than in 2-D flow-through systems. The heterogeneity of the medium does not decrease the compound-specific effects on transverse mixing, which is of particular relevance for reactive solute transport.

In natural aquifers and consolidated rocks, the complex shape, architecture, and connectivity of high-conductivity zones can lead to additional mixing-enhancement mechanisms [e.g., *Stauffer*, 2007; *Chiogna et al*., 2014, 2015; *Cirpka et al*., 2015] and complex pore-scale mixing dynamics [e.g., *Bijeljic et al*., 2013; *Scheven et al*., 2014], which have not been investigated in this study. However, the difference between two-dimensional and three-dimensional mixing enhancement emerging from this analysis points to the need of considering fully three-dimensional geological structures in order to correctly describe mixing enhancement also at the field scale.

Despite the simple geometry of the heterogeneity used in the present study, we have been able to show that the dimensionality of the system and diffusion strongly influence transverse mixing and its enhancement. Such physical processes are fundamental mechanisms for mixing in porous media and therefore will contribute also to mixing of plumes at the larger field scale. Furthermore, we have shown that the outcomes derived from mixing studies focusing on two-dimensional simulations often performed with a simplified parameterization of the dispersion tensor, should be carefully extrapolated to the field scale. In more complex setups with multiple and randomly located inclusions the mixing enhancement will depend on the statistical properties of the field, on the geometric characteristic of the source, on the local dispersion coefficient, on the connectivity of the inclusions as well as on anisotropy of the formation.

Acknowledgments
Experimental data on the flux-related dilution index are provided in Tables 2–7. The values of the concentration measurements at the outlet ports of the 3-D setups used in Figures 6 and 7 are available in the supporting information. This study was supported by the DFG (Deutsche Forschungsgemeinschaft, grants RO 4169/3-1 and CI-26/11-1).

References

Annable, M. D., K. Hatfield, J. Cho, H. Klammer, B. L. Parker, J. A. Cherry, and P. S. C. Rao (2005), Field-scale evaluation of the passive flux-meter for simultaneous measurement of groundwater and contaminant fluxes, *Environ. Sci. Technol.*, *39*(18), 7194–7201, doi:10.1021/es050074g.

Anneser, B., F. Einsiedl, R. U. Meckenstock, L. Richters, F. Wisotzky, and C. Griebler (2008), High-resolution monitoring of biogeochemical gradients in a tar oil-contaminated aquifer, *Appl. Geochem.*, *23*(6), 1715–1730, doi:10.1016/j.apgeochem.2008.02.003.

Atkins, P. W. (1990), *Physical Chemistry*, Oxford Univ. Press, Oxford, U. K.

Bauer, R. D., M. Rolle, P. Kürzinger, P. Grathwohl, R. U. Meckenstock, and C. Griebler (2009). Two-dimensional flow-through microcosms—Versatile test systems to study biodegradation processes in porous aquifers, *J. Hydrol.*, *369*(3–4), 284–295, doi:10.1016/j.jhydrol.2009.02.037.

Bear, J. (1972), *Dynamics of Fluids in Porous Media*, Dover, N. Y.

Bear, J., and Y. Bachmat (1967), A generalized theory on hydrodynamic dispersion in porous media, in *IASH Symposium on Artificial Recharge and Management of Aquifers, IASH Publ.* 72, pp. 7–16, Int. Union Geod. Geophys., Haifa, Israel.

Bijeljic, B., and M. J. Blunt (2007), Pore-scale modelling of transverse dispersion in porous media, *Water Resour. Res.*, *43*, W12S11, doi:10.1029/2006WR005700.

Bijeljic, B., A. Raeini, P. Mostaghimi, and M. J. Blunt (2013), Predictions of non-Fickian solute transport in different classes of porous media using direct simulation on pore-scale images, *Phys. Rev. E*, *87*, 013011, doi:10.1103/PhysRevE.87.013011.

Bjerg, P. L., N. Tuxen, L. A. Reitzel, H. J. Albrechtsen, and P. Kjeldsen (2011), Natural attenuation processes in landfill leachate plumes at three Danish sites, *Ground Water*, *49*(5), 688–705, doi:10.1111/j.1745-6584.2009.00613.x.

Carsel, R. F., and R. S. Parrish (1988), Developing joint probability distributions of soil water retention characteristics, *Water Resour. Res.*, *24*(5), 755–769.

Castro-Alcala, E., D. Fernandez-Garcia, J. Carrera, and D. Bolster (2012), Visualization of mixing processes in a heterogeneous sand box aquifer, *Environ. Sci. Technol.*, *46*(6), 3228–3235, doi:10.1021/es201779p.

Chen, Q., W. Kinzelbach, and S. Oswald (2002), Nuclear magnetic resonance imaging for studies of flow and transport in porous media, *J. Environ. Qual.*, *31*(2), 477–486.

Chiogna, G., and A. Bellin (2013), Analytical solution for reactive solute transport considering incomplete mixing within a reference elementary volume, *Water Resour. Res.*, *49*, 2589–2600, doi:10.1002/wrcr.20200.

Chiogna, G., C. Eberhardt, P. Grathwohl, O. A. Cirpka, and M. Rolle (2010), Evidence of compound-dependent hydrodynamic and mechanical transverse dispersion by multitracer laboratory experiments, *Environ. Sci. Technol.*, *44*(2), 688–693, doi:10.1021/es9023964.

Chiogna, G., O. A. Cirpka, P. Grathwohl, and M. Rolle (2011a), Transverse mixing of conservative and reactive tracers in porous media: Quantification through the concepts of flux-related and critical dilution indices, *Water Resour. Res.*, *47*, W02505, doi:10.1029/2010WR009608.

Chiogna, G., O. A. Cirpka, P. Grathwohl, and M. Rolle (2011b), Relevance of local compound-specific transverse dispersion for conservative and reactive mixing in heterogeneous porous media, *Water Resour. Res.*, *47*, W07540, doi:10.1029/2010WR010270.

Chiogna, G., D. L. Hochstetler, A. Bellin, P. K. Kitanidis, and M. Rolle (2012), Mixing, entropy and reactive solute transport, *Geophys. Res. Lett.*, *39*, L20405, doi:10.1029/2012GL053295.

Chiogna, G., M. Rolle, A. Bellin, and O. A. Cirpka (2014), Helicity and flow topology in three-dimensional anisotropic porous media, *Adv. Water Resour.*, *73*, 134–143, doi:10.1016/j.advwatres.2014.06.017.

Chiogna, G., O. A. Cirpka, M. Rolle, and A. Bellin (2015), Helical flow in three-dimensional non-stationary anisotropic heterogeneous porous media, *Water Resour. Res.*, *51*, 261–280, doi:10.1002/2014WR015330.

Cirpka, O. A., and S. Attinger (2003), Effective dispersion in heterogeneous media under random transient flow conditions, *Water Resour. Res.*, *39*(9), 1257, doi:10.1029/2002WR001931.

Cirpka, O. A., E. O. Frind, and R. Helmig (1999), Numerical simulation of biodegradation controlled by transverse mixing, *J. Contam. Hydrol.*, *40*(2), 159–182, doi:10.1016/S0169-7722(99)00044-3.

Cirpka, O. A., A. Olsson, Q. Ju, M. A. Rahman, and P. Grathwohl (2006), Determination of transverse dispersion coefficients from reactive plume lengths, *Ground Water*, *44*(2), 212–221, doi:10.1111/j.1745-6584.2005.00124.x.

Cirpka, O. A., F. P. J. de Barros, G. Chiogna, M. Rolle, and W. Nowak (2011), Stochastic flux-related analysis of transverse mixing in two-dimensional heterogeneous porous media, *Water Resour. Res.*, *47*, W06515, doi:10.1029/2010WR010279.

Cirpka, O. A., M. Rolle, G. Chiogna, F. P. de Barros, and W. Nowak (2012), Stochastic evaluation of mixing-controlled steady-state plume lengths in two-dimensional heterogeneous domains, *J. Contam. Hydrol.*, *138–139*, 22–39, doi:10.1016/j.jconhyd.2012.05.007.

Cirpka, O. A., G. Chiogna, M. Rolle, and A. Bellin (2015), Transverse mixing in three-dimensional non-stationary anisotropic heterogeneous porous media, *Water Resour. Res.*, *51*, 241–260, doi:10.1002/2014WR015331.

Danquigny, C., P. Ackerer, and J. P. Carlier (2004), Laboratory tracer tests on three-dimensional reconstructed heterogeneous porous media, *J. Hydrol.*, *294*(1–3), 196–212, doi:10.1016/j.jhydrol.2004.02.008.

Davis, G. B., C. Barber, T. R. Power, J. Thierrin, B. M. Patterson, J. L. Rayner, and Q. Wu (1999), The variability and intrinsic remediation of a BTEX plume in anaerobic sulphate-rich groundwater, *J. Contam. Hydrol.*, *36*, 265–290, doi:10.1016/S0169-7722(98)00148-X.

de Anna, P., J. Jimenez-Martinez, H. Tabuteau, R. Turuban, T. Le Borgne, M. Derrien, and Y. Meheust (2014), Mixing and reaction kinetics in porous media: An experimental pore scale quantification, *Environ. Sci. Technol.*, *48*(1), 508–516, doi:10.1021/es403105b.

de Barros, F. P. J., M. Dentz, J. Koch, and W. Nowak (2012), Flow topology and scalar mixing in spatially heterogeneous flow fields, *Geophys. Res. Lett.*, *39*, L08404, doi:10.1029/2012GL051302.

de Dreuzy, J. R., J. Carrera, M. Dentz, and T. Le Borgne (2012), Time evolution of mixing in heterogeneous porous media, *Water Resour. Res.*, *48*, W06511, doi:10.1029/20110078011360.

Dentz, M., and J. Carrera (2003), Effective dispersion in temporally fluctuating flow through a heterogeneous medium, *Phys. Rev. E*, *68*(3), 036310, doi:10.1103/PhysRevE.68.036310.

Devlin, J. F., P. C. Schilling, I. Bowen, C. E. Critchley, D. L. Rudolph, N. R. Thomson, G. P. Tsoflias, and J. A. Roberts (2012), Applications and implications of direct groundwater measurement at the centimetre scale, *J. Contam. Hydrol.*, *127*(1–4), 3–14, doi:10.1016/j.jconhyd.2011.06.007.

Fetter, C. W. (2000), *Applied Hydrogeology*, Prentice Hall, Upper Saddle River, N. J.

Haberer, C. M., M. Rolle, S. Liu, O. A. Cirpka, and P. Grathwohl (2011), A high-resolution non-invasive approach to quantify oxygen transport across the capillary fringe and within the underlying groundwater, *J. Contam. Hydrol.*, *122*(1–4), 26–39, doi:10.1016/j.jconhyd.2010.10.006.

Haberer, C. M., M. Rolle, O. A. Cirpka, and P. Grathwohl (2012), Oxygen transfer in a fluctuating capillary fringe, *Vadose Zone J.*, *11*(3), doi:10.2136/vzj2011.0056.

Haberer, C. M., O. A. Cirpka, M. Rolle, and P. Grathwohl (2014), Experimental sensitivity analysis of oxygen transfer in the capillary fringe, *Ground Water*, *52*(1), 37–49, doi:10.1111/gwat.12028.

Haberer, C. M., M. Rolle, O. A. Cirpka, and P. Grathwohl (2015), Impact of heterogeneity on oxygen transfer in a fluctuating capillary fringe, *Ground Water*, *53*(1), 57–70, doi:10.1111/gwat.12149.

Ham, P. A. S., R. J. Schotting, H. Prommer, and G. B. Davis (2004), Effects of hydrodynamic dispersion on plume lengths for instantaneous bimolecular reactions, *Adv. Water Resour.*, *27*(8), 803–813, doi:10.1016/j.aadvwatres.2004.05.008.

Hazen, A. (1892), Some physical properties of sands and gravels with special reference to their use in filtration, in *24th* Annual Report, Mass. State Board Health, pp. 541–556, Mass.

Heinz, J., and T. Aigner (2003), Three-dimensional GPR analysis of various Quaternary gravel-bed braided river deposits (southwestern Germany), in *Ground Penetrating Radar in Sediments*, vol. 211, edited by C. Bristow and H. Jol, pp. 99–110, Spec. Publ. Geol. Soc., London, U. K.

Herrera, P. A., and A. J. Valocchi (2006), Positive solution of two-dimensional solute transport in heterogeneous aquifers, *Ground Water*, *44*(6), 803–813, doi:10.1111/j.1745-6584.2006.00154.x.

Herrera, P. A., A. J. Valocchi, and R. D. Beckie (2010), A multidimensional streamline-based method to simulate reactive solute transport in heterogeneous porous media, *Adv. Water Resour.*, *33*(7), 711–727, doi:10.1016/j.advwatres.2010.03.001.

Hochstetler, D. L., M. Rolle, G. Chiogna, C. M. Haberer, P. Grathwohl, and P. K. Kitanidis (2013), Effects of compound-specific transverse mixing on steady-state reactive plumes: Insights from pore-scale simulations and Darcy-scaly experiments, *Adv. Water Resour.*, *54*, 1–10, doi:10.1016/j.advwatres.2012.12.007.

Kitanidis, P. K. (1994), The concept of dilution index, *Water Resour. Res.*, *30*(7), 2011–2026, doi:10.1029/94WR00762.

Klenk, I. D., and P. Grathwohl (2002), Transverse vertical dispersion in groundwater and the capillary fringe, *J. Contam. Hydrol.*, *58*(1–2), 111–128, doi:10.1016/S0169-7722(02)00011-6.

Knutson, C., A. Valocchi, and C. Werth (2007), Comparison of continuum and pore-scale models of nutrient biodegradation under transverse mixing conditions, *Adv. Water Resour.*, *30*(6–7), 1421–1431, doi:10.1016/j.advwatres.2006.05.012.

Le Borgne, T., M. Dentz, and E. Villermaux (2013), Stretching, coalescence, and mixing in porous media, *Phys. Rev. Lett.*, *110*(20), 204501, doi:10.1103/PhysRevLett.110.204501.

Lerner, D. N., S. F. Thornton, M. J. Spence, S. A. Banwart, S. H. Bottrell, J. J. Higgo, H. E. H. Mallinson, R. W. Pickup, and G. M. Williams (2000), Ineffective natural attenuation of degradable organic compounds in a phenol-contaminated aquifer, *Ground Water*, *38*(6), 922–928, doi:10.1111/j.1745-6584.2000.tb00692.x.

Liedl, R., A. J. Valocchi, P. Dietrich, and P. Grathwohl (2005), Finiteness of steady state plumes, *Water Resour. Res.*, *41*, W12501, doi:10.1029/2005WR004000.

Liedl, R., P. K. Yadav, and P. Dietrich (2011), Length of 3-D mixing-controlled plumes for a fully penetrating contaminant source with finite width, *Water Resour. Res.*, *47*, W08602, doi:10.1029/2010WR009710.

Mace, R. E., R. S. Fisher, D. Welch, and S. Parra (1997), Extent, mass, and duration of hydrocarbon plumes from leaking petroleum storage tank sites in Texas, *Geol. Circ. 97-1*, Bur. of Econ. Geol., Univ. of Tex., Austin.

Maier, U., and P. Grathwohl (2006), Numerical experiments and field results on the size of steady state plumes, *J. Contam. Hydrol.*, *85*(1–2), 33–52, doi:10.1016/j.jconhyd.2005.12.012.

Marica, F., S. A. Jofre, K. U. Mayer, B. J. Balcom, and T. A. Al (2011), Determination of spatially-resolved porosity, tracer distributions and diffusion coefficients in porous media using MRI measurements and numerical simulations, *J. Contam. Hydrol.*, *125*(1–4), 47–56, doi:10.1016/j.jconhyd.2011.04.008.

Mayer, K. U., S. G. Benner, E. O. Frind, S. F. Thornton, and D. N. Lerner (2001), Reactive transport modeling of processes controlling the distribution and natural attenuation of phenolic compounds in a deep sandstone aquifer, *J. Contam. Hydrol.*, *53*(3–4), 341–368, doi:10.1016/S0169-7722(01)00173-5.

McCray, J. E., and R. W. Falta (1997), Numerical simulation of air sparging for remediation of NAPL contamination, *Ground Water*, *35*(1), 99–110, doi:10.1111/j.1745-6584.1997.tb00065.x.

Oswald, S., W. Kinzelbach, A. Greiner, and G. Brix (1997), Observation of flow and transport processes in artificial porous media via magnetic resonance imaging in three dimensions, *Geoderma*, *80*(3–4), 417–429, doi:10.1016/S0016-7061(97)00064-5.

Oswald, S. E., and W. Kinzelbach (2004), Three-dimensional physical benchmark experiments to test variable-density flow models, *J. Hydrol.*, *290*(1–2), 22–42, doi:10.1016/j.jhydrol.2003.11.037.

Pedretti, D., D. Fernandez-Garcia, D. Bolster, and X. Sanchez-Vila (2013), On the formation of breakthrough curves tailing during convergent flow tracer tests in three-dimensional heterogeneous aquifers, *Water Resour. Res.*, *49*, 4157–4173, doi:10.1002/wrcr.20330.
Pollock, D. W. (1988), Semianalytical computation of path lines for finite-difference models, *Ground Water*, *26*(6), 743–750, doi:10.1111/j.1745-6584.1988.tb00425.x.
Porta, G. M., S. Chaynikov, J. Thovert, M. Riva, A. Guadagnini, and P. M. Adler (2013), Numerical investigation of pore and continuum scale formulations of bimolecular reactive transport in porous media, *Adv. Water Resour.*, *62*, 243–253, doi:10.1016/j.advwatres.2013.09.007.
Prommer, H., N. Tuxen, and P. Bjerg (2006), Fringe-controlled natural attenuation of phenoxy acids in a landfill plume: Integration of field-scale processes by reactive transport modeling, *Environ. Sci. Technol.*, *40*, 4732–4738, doi:10.1021/es0603002.
Prommer, H., B. Anneser, M. Rolle, F. Einsiedl, and C. Griebler (2009), Biogeochemical and isotopic gradients in a BTEX/PAH contaminant plume: Model-based interpretation of a high-resolution field data set, *Environ. Sci. Technol.*, *43*, 8206–8212, doi:10.1021/es901142a.
Rahman, M. A., S. C. Jose, W. Nowak, and O. A. Cirpka (2005), Experiments on vertical transverse mixing in a large-scale heterogeneous model aquifer, *J. Contam. Hydrol.*, *80*(3–4), 130–148, doi:10.1016/j.jconhyd.2005.06.010.
Rashidi, M., L. Peurrung, A. F. B. Tompson, and T. J. Kulp (1996), Experimental analysis of pore-scale flow and transport in porous media, *Adv. Water Resour.*, *19*(3), 163–180, doi:10.1016/0309-1708(95)00048-8.
Renard, P., and D. Allard (2013), Connectivity metrics for subsurface flow and transport, *Adv. Water Resour.*, *51*, 168–196, doi:10.1016/j.advwatres.2011.12.001.
Rolle, M., and P. K. Kitanidis (2014), Effects of compound-specific dilution on transient transport and solute breakthrough: A pore-scale analysis, *Adv. Water Resour.*, *71*, 186–199, doi:10.1016/j.advwatres.2014.06.012.
Rolle, M., C. Eberhardt, G. Chiogna, O. A. Cirpka, and P. Grathwohl (2009), Enhancement of dilution and transverse reactive mixing in porous media: Experiments and model-based interpretation, *J. Contam. Hydrol.*, *110*(3–4), 130–142, doi:10.1016/j.jconhyd.2009.10.003.
Rolle, M., D. L. Hochstetler, G. Chiogna, P. K. Kitanidis, and P. Grathwohl (2012), Experimental investigation and pore-scale modeling interpretation of compound-specific transverse dispersion in porous media, *Transp. Porous Media*, *93*(3), 347–362, doi:10.1007/s11242-012-9953-8.
Rolle, M., M. Muniruzzaman, C. M. Haberer, and P. Grathwohl (2013a), Coulombic effects in advection-dominated transport of electrolytes in porous media: Multicomponent ionic dispersion, *Geochim. Cosmochim. Acta*, *120*, 195–205, doi:10.1016/j.gca.2013.06.031.
Rolle, M., G. Chiogna, D. L. Hochstetler, and P. K. Kitanidis (2013b), On the importance of diffusion and compound-specific mixing for groundwater transport: An investigation from pore to field scale, *J. Contam. Hydrol.*, *153*, 51–68, doi:10.1016/j.jconhyd.2013.07.006.
Scheven, U. M. (2013), Pore-scale mixing and transverse dispersivity of randomly packed monodisperse spheres, *Phys. Rev. Lett.*, *110*, 214504, doi:10.1103/PhysRevLett.110.214504.
Scheven, U. M., S. Khirevich, A. Daneyko, and U. Tallarek (2014), Longitudinal and transverse dispersion in flow through random packings of spheres: A quantitative comparison of experiments, simulations, and models, *Phys. Rev. E*, *89*, 053023, doi:10.1103/PhysRevE.89.053023.
Silliman, S. E. (1996), The importance of the third dimension on transport through saturated porous media: Case study based on transport of particles, *J. Hydrol.*, *179*(1–4), 181–195, doi:10.1016/0022-1694(95)02838-2.
Stauffer F. (2007), Impact of highly permeable sediment units with inclined bedding on solute transport in aquifers, *Adv. Water Resour.*, *30*, 2194–2201, doi:10.1016/j.advwatres.2007.04.008.
Tartakovsky, A. M., G. D. Tartakovsky, and T. D. Scheibe (2009), Effects of incomplete mixing on multicomponent reactive transport, *Adv. Water Resour.*, *32*(11), 1674–1679, doi:10.1016/j.advwatres.2009.08.012.
Thornton, S. F., S. Quigley, M. J. Spence, S. A. Banwart, S. Bottrell, and D. N. Lerner (2001), Process controlling the distribution and natural attenuation of dissolved phenolic compounds in a deep sandstone aquifer, *J. Contam. Hydrol.*, *53*, 233–267, doi:10.1016/S0169-7722(01)00168-1.
van der Kamp, G., L. D. Luba, J. A. Cherry, and H. Maathuis (1994), Field study of a long and very narrow contaminant plume, *Ground Water*, *32*(6), 1008–1016, doi:10.1111/j.1745-6584.1994.tb00940.x.
van Genuchten, M. T. (1980), A closed-form equation for predicting the hydraulic conductivity in unsaturated soils, *Soil Sci. Soc. Am. J.*, *44*(5), 892–898, doi:10.2136/sssaj1980.03615995004400050002x.
Werth, C. J., O. A. Cirpka, and P. Grathwohl (2006), Enhanced mixing and reaction through flow focusing in heterogeneous porous media, *Water Resour. Res.*, *42*, W12414, doi:10.1029/2005WR004511.
Wexler, E. J. (1992), Analytical solutions for one-, two-, and three-dimensional solute transport in ground-water flow systems with uniform flow, in *Applications of Hydraulics*, vol. 3, chap. B7, U.S. Geol. Surv., N. Y.
Wiedemeier, T. H., H. S. Rifai, C. J. Newell, and J. T. Wilson (1999), *Natural Attenuation and Fuels and Chlorinated Solvents in the Subsurface*, John Wiley, Hoboken, N. J.
Willingham, T. W., C. J. Werth, and A. J. Valocchi (2008), Evaluation of the effects of porous media structure on mixing-controlled reactions using pore-scale modeling and micromodel experiments, *Environ. Sci. Technol.*, *42*(9), 3185–3193, doi:10.1021/es7022835.
Worch, E. (1993), A new equation for the calculation of diffusion coefficients for dissolved substances, *Vom Wasser*, *81*, 289–297.
Ye, Y., G. Chiogna, O. A. Cirpka, P. Grathwohl, and M. Rolle (2015), Experimental investigation of compound-specific dilution of solute plumes in saturated porous media: 2-D vs. 3-D flow-through systems, *J. Contam. Hydrol.*, *172*, 33–47, doi:10.1016/j.jconhyd.2014.11.002.
Yoon, H., and S. A. McKenna (2012), Highly parameterized inverse estimation of hydraulic conductivity and porosity in a three-dimensional, heterogeneous transport experiment, *Water Resour. Res.*, *48*, W10536, doi:10.1029/2012WR012149.
Zarlenga, A., and A. Fiori (2013), Steady plumes in heterogeneous porous formations: A stochastic Lagrangian approach, *Water Resour. Res.*, *49*, 864–873, doi:10.1002/wrcr.20106.
Zarlenga, A., and A. Fiori (2014), Stochastic analytical modeling of the biodegradation of steady plumes, *J. Contam. Hydrol.*, *157*, 106–116, doi:10.1016/j.jconhyd.2013.11.003.